Dynamic Load Environment of Bridge-Mounted Sign Support Structures

Bartlomiej Zalewski & Arthur Huckelbridge

Report No. **ST/SS/05-002** for the
Ohio Department of Transportation
Office of Research and Development

State Job Number 134153

September, 2005

CASE
CASE WESTERN RESERVE UNIV

FHWA

RESEARCH & DEVELOPMENT

1. Report No. ST/SS/05-002	2. Government Accession No.	3. Recipient's Catalog No.

4. Title and subtitle. **Dynamic Load Enviornment of Bridge Mounted Sign Support Structures**	5. Report Date **September 2005**
	6. Performing Organization Code
7. Author(s) **Dr. Art Huckelbridge** **Mr. Bart Zalewski**	8. Performing Organization Report No.
9. Performing Organization Name and Address **Case Western Reserve University** **Department of Civil Engineering** **10900 Euclid Avenue** **Cleveland, Ohio 44106**	10. Work Unit No. (TRAIS)
	11. Contract or Grant No. **State Job No. 134153**
	13. Type of Report and Period Covered Final Report
12. Sponsoring Agency Name and Address Ohio Department of Transportation 1980 W Broad Street Columbus, OH 43223	14. Sponsoring Agency Code

15. Supplementary Notes

16. Abstract

An investigation was conducted into the failure of a welded aluminum truss sign support structure on an existing interstate highway bridge. The investigation was conducted in three main steps; 1) fatigue testing in the laboratory of surviving segments of the failed sign, 2) collection of dynamic response data of the identical replacement structure in situ, and 3) finite element modeling and simulation of the bridge and truss structural system.

The welded aluminum space truss indicated a typical fatigue failure, with a fatigue crack initiating at a welded chord/diagonal connection detail (AASHTO fatigue category ET; CAFL = .44 ksi). Fatigue testing in the laboratory of surviving segments of the structure produced an identical fatigue failure at a similar location after 3,000,000 load cycles at a 1 ksi stress range. Field monitoring of acceleration data at three different locations of the in-situ truss was conducted in order to characterize the dynamic behavior of the truss and the bridge structural system. A finite element model of a segment of the multi-span bridge which included the mounting location of the sign support truss, was assembled.

In the modeling of the truss a moving traffic load, consisting of a single truck, was considered. A modal time history analysis for moving vehicle loads was performed. The analysis results indicated that the failure was a classical fatigue rupture, induced primarily by the dynamic effect of moving truck traffic on the bridge. Even though inferred cyclic stress levels were well below the CAFL for the detail in question, the extremely high number of low amplitude traffic-induced stress cycles (in the hundreds of millions), combined with the absence of an endurance limit for welded aluminum, resulted in the observed failure. (A typical truck passage resulted in roughly 75 stress cycles in the truss, due to the low damping and extended time of vibration decay.) The predicted lifetime of the replacement sign support structure is approximately that exhibited by the original structure, namely thirty to forty years.

17. Key Words aluminum, welding, fatigue failures, sign support structures		18. Distribution Statement No Restrictions. This document is available to the public through the National Technical Information Service, Springfield, Virginia 22161	
19. Security Classif. (of this report) Unclassified	20. Security Classif. (of this page) Unclassified	21. No. of Pages	22. Price

Form DOT F 1700.7 (8-72) Reproduction of completed page authorized

TABLE OF CONTENTS

LIST OF TABLES

LIST OF FIGURES

Figure Page

Failure Analysis of a Bridge-Mounted Sign Support Truss

Abstract

by

Bartlomiej Franciszek Zalewski

An investigation was conducted into the failure of a welded aluminum truss sign support structure on an existing interstate highway bridge. The investigation was conducted in three main steps; 1) fatigue testing in the laboratory of surviving segments of the failed sign, 2) collection of dynamic response data of the identical replacement structure in situ, and 3) finite element modeling and simulation of the bridge and truss structural system.

The welded aluminum space truss indicated a typical fatigue failure, with a fatigue crack initiating at a welded detail. Fatigue testing in the laboratory of surviving segments of the structure produced an identical fatigue failure at a similar location after 3,000,000 load cycles. Field monitoring of acceleration data at three different locations of the in-situ truss was conducted in order to characterize the dynamic behavior of the truss and the bridge structural system. A finite element model of a segment of the multi-span bridge which includes the location of the sign support truss, was assembled.

In the modeling of the truss two external loading conditions, namely traffic load and wind load, were considered. It was presumed that these two load sources were most likely to produce dynamic response in the bridge/sign truss structural system. Both modal analysis and time history analysis for moving vehicle loads were performed. The

analysis results indicated that the failure was a classical fatigue rupture, induced primarily by the dynamic effect of moving truck traffic on the bridge. The predicted lifetime of the replacement sign support structure is approximately that exhibited by the original structure, namely thirty to forty years.

Chapter I

Introduction

1.1 Background and Objectives

Aluminum sign support trusses have been used by various departments of transportation since the early 1960's. In that time, a number of them have exhibited fracture failures in various elements, with the most likely cause being fatigue rupture due to wind-induced vibrations. The observed cracks typically initiate at the welded joints between the branch and chord members and propagate circumferentially. These cracks can cause result in failure of the main members or of the total structure and endanger the passing traffic. To overcome the possibility of failure, some prevention efforts have been undertaken. For instance, glass fiber reinforced polymer composites are being investigated to arrest the propagation of the crack and to ensure the proper performance of connections. However, such repair requires the identification of the existing crack and therefore is practically impossible to achieve in a timely fashion in every truss. Thus more refined analyses of such trusses and their load environments is necessary to design them reliably.

The truss considered in this investigation experienced a fracture failure that occurred much earlier than the expected lifetime. The current design specifications for highway sign trusses by American Association of State Highways and Transportation Officials (AASHTO), from 1985, consider only wind load, as the failures are mostly characterized as fatigue rupture caused by wind induced vibrations, particularly for cantilever structures.

Bridge-type trusses, particularly when mounted on a bridge, have the potential for significant levels of traffic induced vibrations. The objectives of this investigation were to determine the cause of the fracture failure of this particular sign support truss, and to make any indicated recommendations as to future fatigue considerations warranted for this type of structure.

1.2 Overview

Chapter I provides an historical background of fracture failures and describes the physical characteristics of the truss under investigation. Chapter II details the truss failure examination and preliminary concepts of the possible reason for failure, including laboratory fatigue testing of portions of the failed structure. This chapter also describes the field monitoring that was performed, in order to obtain adequate data such that the dynamic properties of the truss could be inferred. Chapter III introduces the finite element model that is used in the investigation. Chapter IV contains the results of the finite element analysis and correlates results with the field data. It also provides conclusions as well as recommendations to improve conceptual design.

1.3 Historical Background

Fracture failure has been observed to occur in structures, even though the strength design requirement was satisfied. Before World War II in Europe, fracture failures were detected in several truss bridges despite no unusual loading conditions and a low temperature variation. Investigation showed that the main cause of the bridge failure was a crack initiation from a weld defect. These welds were observed to contain discontinuities.

By 1946, more than 20% of the merchant ships were observed to develop cracks of significant size. Between 1942 and 1952 over 200 ships were classified as having serious fractures including nine T-2 tankers and seven Liberty ships that failed as a result of a fracture. The majority of failures that occurred in T-2 tankers were caused by a defect in the bottom-shell butt welds.

In 1950's fracture failures still occurred in ships despite design improvements. Between 1951 and 1953, two relatively new all-welded cargo ships as well as a transversely framed tanker broke in two. Between 1960 and 1965, ten fracture failures occurred in welded ships. In 1972 a 584-foot long Tank Barge I.O.S. 3301 suddenly broke in two due to improper ballasting while it was in port.

In 1962, the Kings Bridge in Melbourne failed because of fracture due to poor detail design and fabrication errors, which resulted in cracks that nearly propagated through the entire flange prior to any service loads. The bridge-building industry started paying more attention to fracture failures after the failure of Point Pleasant Bridge, in West Virginia. In 1967 this bridge collapsed without any warning. Since then, other fracture failures had occurred in steel bridges due to fabrication errors, faults in detail design, or material properties.

On some frame structures failure occurs due to fatigue. One particular case (Jones 1998) that was studied involved a steel leg press bench that failed due to fatigue fracture which originated at the circumferential fillet weld connecting the post to the rectangular cross frame member. The visual examination of the weld showed a lamellar tear revealing the poor quality of the weld. The fracture originated not only at the root but also on the face of the weld, since higher stress concentration occurred at the face of the weld because of the poor weld quality.

1.4 Previous Work

Previous studies have been made to improve the reliability of cantilever sign supports. The main difference between a cantilever sign support and an overhead sign support truss, like the one studied in this work, is its higher flexibility. Cantilever structures therefore tend to exhibit a low circular fundamental frequency. Due to a low damping ratio, combined with a low frequency, these cantilever support structures are most often affected by wind-induced vibrations. Updated fatigue-resistant design requirements (Kaczinski et al 1996) were initiated that consider an amplified equivalent static pressure, which is a conservative representation of the dynamic wind load. However, vibrations due to support movements, such as those due to traffic load, are not generally considered in the design requirements.

Chapter II

The Failed Structure and Its Supporting Bridge

2.1 Bridge Description

The location of the investigated truss is in District 12 of Ohio Department of Transportation (ODOT), at the interstate route 77 / interstate route 480 interchange, on bridge no. CUY-77-0952. The bridge upon which the failed sign truss was mounted spans southbound over the Cuyahoga River Valley, and consists of 25 spans with a total length of 3,023 ft. The sign was located on the fifth span from the south end of the bridge; this span measures 133 ft. The supporting bridge consists of three southbound lanes, from which the right lane merges right onto interstate route 480, the left lane continues on interstate route 77 and the center lane divides into two, with one lane following each of the respective routes. The speed limit on the bridge is 60 mph. The plan layout of the bridge is shown in Figure 2.1

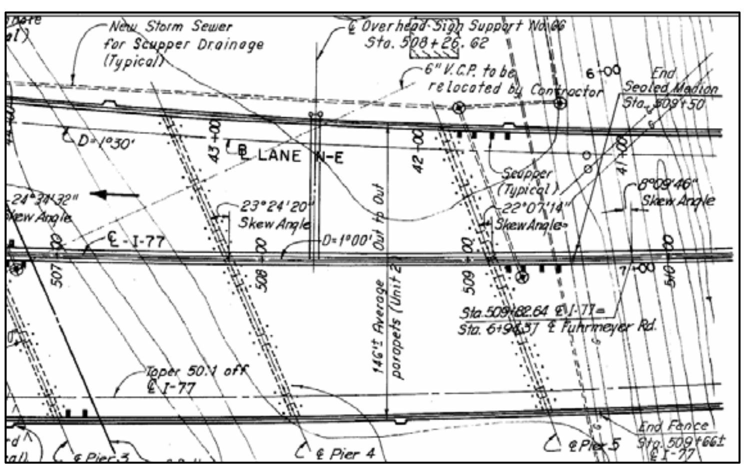

Figure 2.1: Plan layout of the bridge

2.2 Truss Description

The sign support truss is a three dimensional four-chord welded aluminum space truss, spanning 73 ft. The four parallel chords of the truss are placed on a 4ft x 4ft grid. The height from the traffic lanes to the lower cord of the truss is 22 ft. The dismantled truss, following the failure, is shown in Figure 2.2.

Figure 2.2: Failed sign support truss

2.3 Visual Truss Examination

The failed sign support truss was visually examined to determine the possible cause of failure. The location of a fracture was observed to be adjacent to the end of the truss, at the weld between the branch and chord member. This fracture exhibited a typical fatigue rupture surface. The fractured cross-section is divided into two areas from which the failure type can be inferred. The major part, consisting of approximately 75% of the cross section, is the area of crack propagation. In this portion the crack has initiated and slowly propagated along the circumference of the weld. This is inferred from a rough surface on the fractured cross-section which is due to slow material failure, present in a case of fatigue. The second part, consisting of approximately 25% of the cross-section, is characterized by a smooth surface on the fractured cross-section which is due to the instantaneous material failure. The crack propagated circumferentially around the chord member until failure (see Figure 2.3).

Figure 2.3: Fractured truss subjected to cyclic load

2.4 Field Observation

A replacement sign support truss with identical material and geometric properties to the failed truss was installed on the same set of verticals support posts which had supported the failed sign. The new truss was field monitored to obtain necessary data to characterize its dynamic behavior. Three accelerometers were used; two uni-axial accelerometers, PCB model U353B33, and one tri-axial accelerometer, PCB model 356A08. The two uni-axial accelerometers were attached at the base of each of the truss columns and the tri-axial accelerometer was attached at the mid-span of the truss. The uni-axial accelerometers were orientated so as to measure the vertical acceleration. The tri-axial accelerometer was located such that it measured the vertical acceleration, the acceleration parallel to the direction of traffic and the acceleration perpendicular to the direction of traffic. The location of the accelerometers is shown in Figure 2.4.

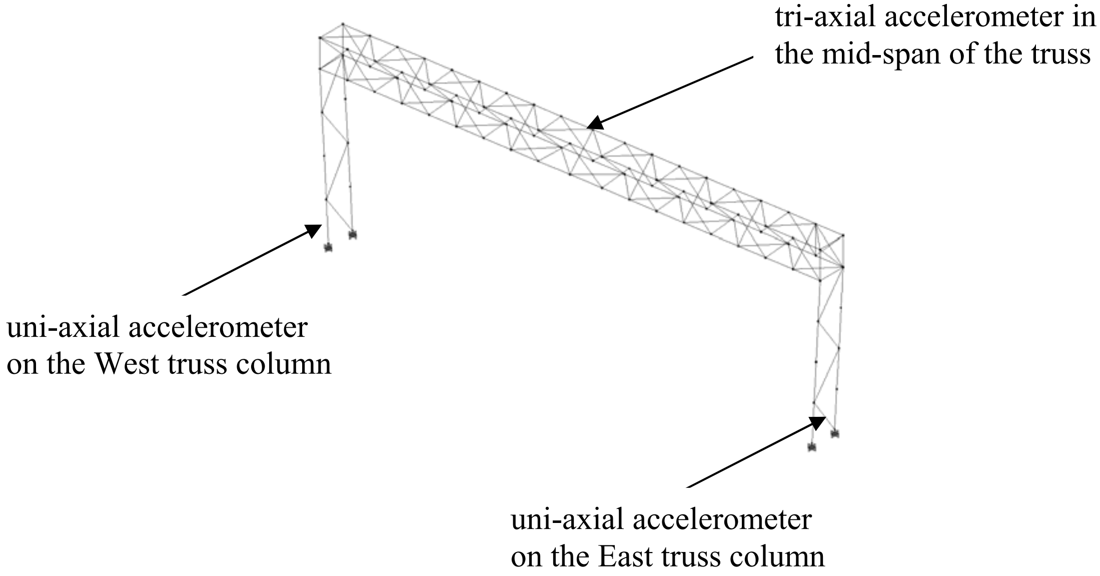

Figure 2.4: Accelerometer locations on the sign support truss

The data was measured during traffic and during several passes of an ODOT District 12 dumptruck, loaded with gravel for an approximate weight of 55,000 pounds (see Figure 2.5). The data was collected using a Campbell Scientific CR9000 Measurement and Control System and Campbell Scientific PC9000 Support Software. Ten data sets were collected for further analysis. This amount of data was deemed sufficient for understanding the dynamic behavior of the truss and its supporting bridge.

Figure 2.5: Truck used for field monitoring

2.5 Field Data Processing

The collected field acceleration data contains noise and a non-monotonic drift due to the imperfections of the accelerometers as well as the connections between the accelerometers and measurement and control system. In order to improve the collected data, a high-pass and a low-pass filtering were performed to separate the actual acceleration experienced by the structure from the measurement imperfections. The filtering procedure was performed using filtering operations imbedded in Matlab software. The program uses the filtering operations with variable $x(t)$ as an input and variable $y(t)$ as an output as described in the following steps.

Output $y(t)$ can be defined as a transformation of the input $x(t)$:

$$y(t) = T[x(t)] \tag{1}$$

Assume a shift invariance:

$$x(t) \rightarrow y(t) \quad \text{then} \quad x(t-k) \rightarrow y(t-k) \tag{2}$$

For a discrete system the output can be obtained by the transformation of the discrete input weighted by a sampling function:

$$y(t) = T[\sum_{k=-\infty}^{\infty} x_k \delta(t-k)] \tag{3}$$

or:

$$y(t) = \sum_{k=-\infty}^{\infty} x_k \cdot T[\delta(t-k)] \tag{4}$$

$T[\delta(t-k)]$ is known as the unit-sample response given as:

$$h(t-k) = T[\delta(t-k)] \tag{5}$$

substitution of Eq. 5 in Eq.4:

$$y(t) = \sum_{k=-\infty}^{\infty} x_k \cdot h(t-k) \tag{6}$$

If $y(t)$ is a sequence whose values are related to two sequences $h(t)$ and $x(t)$, then $y(t)$ is the convolution of $x(t)$ with $h(t)$ given as:

$$y(t) = x(t) * h(t) \tag{7}$$

equating Eq. 6 and Eq. 7:

$$x(t) * h(t) = \sum_{k=-\infty}^{\infty} x_k \cdot h(t-k) \tag{8}$$

or;

$$x(t) * h(t) = \sum_{k=-\infty}^{\infty} h_k \cdot x(t-k) \tag{9}$$

From Eq. 8 and Eq. 9 the following relation can be deduced:

$$\sum_{k=-\infty}^{\infty} x_k \cdot h(t-k) = \sum_{k=-\infty}^{\infty} h_k \cdot x(t-k) \tag{10}$$

Assume $x(t)$ to be harmonic:

$$x(t) = e^{i\omega t} \tag{11}$$

where ω is the circular frequency. Substitution of Eq. 11 and Eq. 10 into Eq. 6:

$$y(t) = \sum_{k=-\infty}^{k=\infty} h(k) \cdot e^{i\omega(t-k)} \tag{12}$$

or:

$$y(t) = e^{i\omega t} \cdot \sum_{k=-\infty}^{k=\infty} h(k) \cdot e^{-i\omega k} \tag{13}$$

The Fourier Series of $h(k)$ can be expressed as:

$$H(e^{i\omega}) = \sum_{k=-\infty}^{k=\infty} h(k) \cdot e^{-i\omega k} \tag{14}$$

Then, Eq. 13:

$$y(t) = H(e^{i\omega}) \cdot e^{i\omega t} \tag{15}$$

By substituting of Eq, 11 into Eq. 14 it is seen that $H(e^{iw})$ is a filtering function between $y(t)$ and $x(t)$:

$$y(t) = H(e^{i\omega}) \cdot x(t) \tag{16}$$

2.6 Z-transformation:

Matlab software uses a similar filtering procedure in z-domain. The z-transform is defined as:

$$X(z) = \sum_{n=-\infty}^{k=\infty} x(n) \cdot z^{-n} \tag{17}$$

where:

$$z = r \cdot e^{i\omega} \tag{18}$$

The notation that will be used to define a z-transform as follows:

$$\text{z-transform of } x(n) = \Im[x(n)] \tag{18}$$

Consider:

$$y(t) = x(t) * h(t) \tag{20}$$

a relation in z-domain can be obtained by taking a z-transform of both sides of Eq. 20:

$$Y(z) = X(z) \cdot H(z) \tag{21}$$

$H(z)$ is the filtering function in z domain between the input $X(z)$ and the response $Y(z)$. Any shift invariant systems can be described by the linear constant-coefficient difference equation:

$$\sum_{k=0}^{L} a_k \cdot y(n-k) = \sum_{u=0}^{M} b_u \cdot x(n-u) \tag{22}$$

Taking the z-transform of Eq. 22:

$$\sum_{k=0}^{L} a_k \cdot z^{-k} \cdot Y(z) = \sum_{u=0}^{M} b_u \cdot z^{-u} \cdot X(z) \tag{23}$$

Using Eq.21:

$$H(z) = \frac{Y(z)}{X(z)} \tag{24}$$

Substituting Eq. 24 into Eq. 23:

$$H(z) = \frac{\sum_{u=0}^{M} b_u \cdot z^{-u}}{\sum_{k=0}^{L} a_k \cdot z^{-k}} \tag{25}$$

Setting $u = k = r - 1$ and letting the filter be of the N$^{\text{th}}$ order, where $M = L = N + 1$, the Eq 25. is modified as:

$$H(z) = \frac{\sum_{r=1}^{N+1} b_r \cdot z^{1-r}}{\sum_{r=1}^{N+1} a_r \cdot z^{1-r}} \tag{26}$$

The first order filtering function is obtained by letting $N = 1$. Eq. 26 then simplifies to the following form:

$$H(z) = \frac{b(1) + b(2) \cdot z^{-1}}{1 + a(2) \cdot z^{-1}} \tag{27}$$

This form of the digital analog filter function is used by Matlab software to obtain the vector of coefficients b and a which are used in the filtering operation. To filter the collected acceleration data two types of filters are used, the high-pass filter and the low-pass filter. The obtained vectors of parameters b and a vary dependent on the type of filter that is desired. Matlab software uses the difference equation to perform filtering operation as described in the following steps. Then Eq. 22 can be rewritten in the following form:

$$a(1)\cdot y(n) = -\sum_{r=2}^{N+1} a_r \cdot y(n-r+1) + \sum_{r=1}^{N+1} b_r \cdot x(n-r+1) \tag{28}$$

Setting $a(1)=1$ and letting N=1 for the first order filter Eq. 28 is modified to the following form:

$$y(n) = b(1)\cdot x(n) + b(2)\cdot x(n-1) - a(2)\cdot y(n-1) \tag{29}$$

In time domain Eq. 29 can be rewritten as:

$$y(t) = b(1)\cdot x(t) + b(2)\cdot x(t-1) - a(2)\cdot y(t-1) \tag{30}$$

where $x(t)$ is the collected discrete acceleration data and $y(t)$ is the filtered acceleration.

2.7 Frequency Analysis of the Field data

2.7.1 Fast Fourier Transform:

The collected acceleration data is used to determine the dynamic properties needed to understand the dynamic response of the structure. The natural frequencies of structures are the one of the essential characteristics describing the structures' behavior when subjected to dynamic load such as earthquake, wind or traffic. Frequency analysis of the obtained data is used to determine the fundamental frequency of the sign support truss and its supporting bridge. The two uni-axial accelerometers measured the vertical bridge response. The data from these accelerometers is used to obtain the fundamental frequencies of the bridge. The tri-axial accelerometer measured the response of the truss in the three directions that were described previously. The data from this accelerometer is used to obtain three fundamental frequencies of the truss in each of these three directions. Due to discontinuities in the data, the frequency analysis procedure is modified to consider the discontinuity. The analysis is performed using Matlab software. The filtered acceleration data was transformed from time domain to frequency domain using Fast Fourier Transform (FFT) adapted to discrete data points. The transformation procedure is explained as following:

The Fourier Transform of the continuous periodic function is given as:

$$X(\omega) = \frac{1}{T} \cdot \int_{-\infty}^{\infty} x(t) \cdot e^{-i\omega t} dt \qquad (31)$$

where ω is the circular frequency and T is a period over time interval that is considered in the limits of integration, which is defined as the time interval between two identical cycles. In a digitized data, unless it consists of a digitized periodic function, the period can be defined as the entire time interval since there is no repetition of cycles. The following variables need to be defined to proceed with the derivation of discrete Fourier Transform or FFT.

$$r = 0,1,...,N-1 \tag{32}$$

$$k = 0,1,...,N-1 \tag{33}$$

N is the total number of collected points, k corresponds to a (k+1)th sample, and r is an index. Then:

$$r \cdot \Delta = t \tag{34}$$

$$N \cdot \Delta = T \tag{35}$$

$$\omega_k = \frac{2\pi \cdot k}{T} = \frac{2\pi \cdot k}{N \cdot \Delta} \tag{36}$$

$$\Delta\omega = \frac{2\pi}{N \cdot \Delta} = \frac{2\pi \cdot f_s}{N} \tag{37}$$

Δ is the sampling time interval, t is the discrete time at which the data was collected, and f_s is the sampling frequency. For a specific circular frequency, the continuous Fourier Transform can be written as:

$$X\ (\omega_k) = \frac{1}{T} \cdot \int_{-\infty}^{\infty} x(t) \cdot e^{-i\omega_k t} dt \tag{38}$$

Eq. 34 and Eq. 36 are substituted into Eq. 38. Eq. 38 is modified with a summation due to discrete time input. These substitutions yield a following formulation:

$$X(\omega_k) = \frac{1}{T} \cdot \sum_{r=0}^{N-1} x_r \cdot e^{\frac{-i2\pi kr}{N}} \Delta \tag{39}$$

Since Δ is a constant Eq. 39 can is written as:

$$X(\omega_k) = \frac{\Delta}{T} \cdot \sum_{r=0}^{N-1} x_r \cdot e^{\frac{-i2\pi kr}{N}} = \frac{1}{N} \cdot \sum_{r=0}^{N-1} x_r \cdot e^{\frac{-i2\pi kr}{N}} \tag{40}$$

2.6.2 Frequency Bounds:

The FFT creates a signal's frequency contribution for all the frequencies separated by $\Delta\omega$. The frequency range that is valid, however, is bounded by $\omega = 0$ and $\omega = \dfrac{\pi}{\Delta}$. The lower bound of the frequency range is due to the symmetry of the frequency contributions about the $\omega = 0$ axis. The symmetry occurs because the frequency contribution is considered as the absolute value of the Fast Fourier Transform since a frequency contribution must be a positive value. The negative frequency contribution does not have a physical meaning, therefore, it is not considered in the analysis. The upper bound is due to the frequency contribution repetition beyond the actual measured frequencies. This is shown in the following proof. Let $k = N + l$ so that Eq. 40 can be rewritten as:

$$X(\omega_{N+l}) = \frac{1}{N} \cdot \sum_{r=0}^{N-1} x_r \cdot e^{\frac{-i2\pi r\cdot(N+l)}{N}} \tag{41}$$

where $l \to 0 - N$. Eq. 41 can be expanded as shown:

$$X\ (\omega_{N+l}) = \frac{1}{N} \cdot \sum_{r=0}^{N-1} x_r \cdot e^{\frac{-i2\pi r\cdot l}{N}} \cdot e^{-i2\pi r} \tag{42}$$

As $r \in \mathscr{I}$, Eq. 42 can be simplified to:

$$X(\omega_{N+l}) = \frac{1}{N} \cdot \sum_{r=0}^{N-1} x_r \cdot e^{\frac{-i2\pi lr}{N}} \tag{43}$$

Letting $k = l$ Eq. 40 is written as:

$$X\ (\omega_l) = \frac{1}{N} \cdot \sum_{r=0}^{N-1} x_r \cdot e^{\frac{-i2\pi lr}{N}} \tag{44}$$

Eq. 43 and Eq. 44 are identical; therefore it is shown that the frequency contribution repeats itself after $\omega = \frac{2\pi}{\Delta}$. The total valid range of frequency for N discrete frequency contributions is given as $\omega = \frac{2\pi}{\Delta}$. Since it has been shown that the symmetry about $\omega = 0$ axis is present, the frequency range must enclose the positive and negative frequency contributions. This requires that the valid frequency range must lie in the interval $\omega \in [-\frac{\pi}{\Delta}, \frac{\pi}{\Delta}]$. Therefore, the unique frequency contribution is bounded within $\omega \in [0, \frac{\pi}{\Delta}]$.

2.8 Frequency Analysis Results

The analysis of the acceleration data determines dynamic behavior of the truss and its supporting bridge. The above described analytical procedures are performed on collected field data using Matlab software and the fundamental frequencies of the bridge and the truss are obtained. A typical procedure is graphically shown below in figures 2.6 through 2.8. Figure 2.6 shows data that was collected from field monitoring; in this example vertical acceleration of the truss.

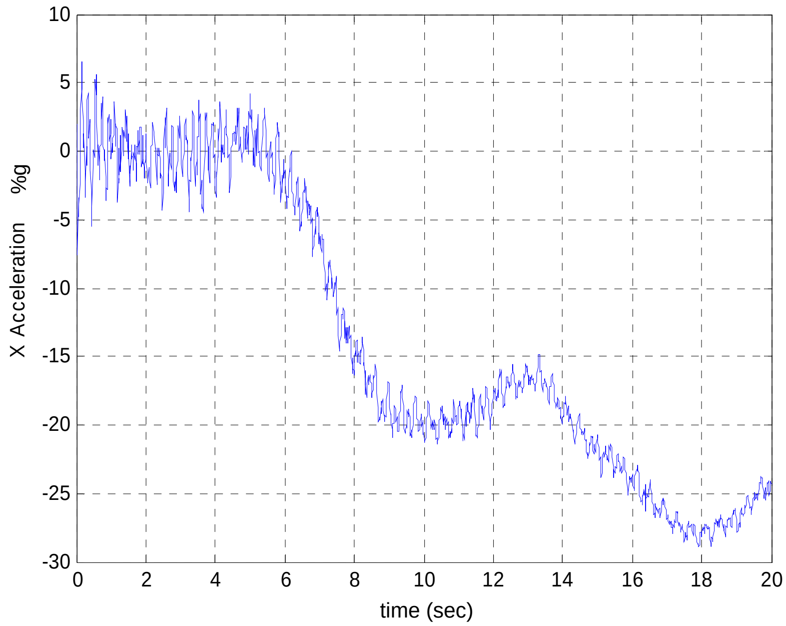

Figure 2.6: Measured acceleration time history

Figure 2.7 shows the same data which was filtered to obtain correct acceleration measure of the structure in question.

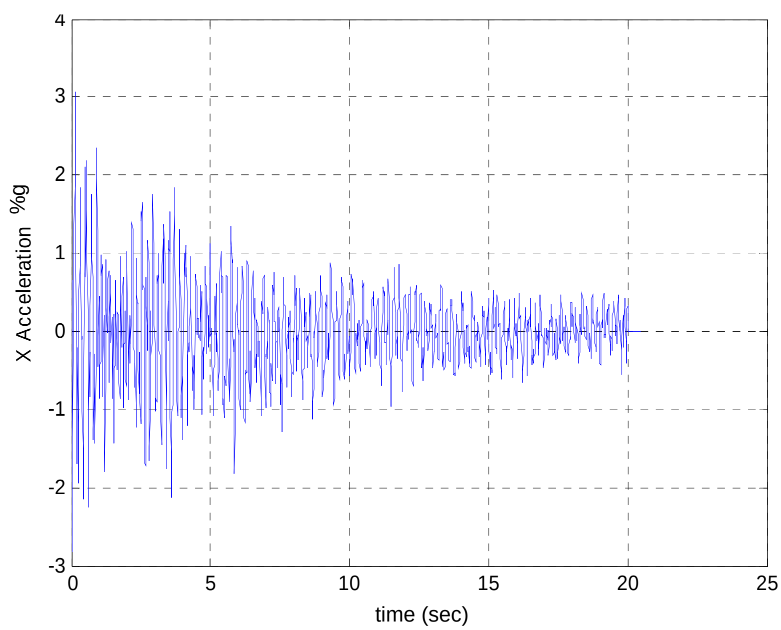

Figure 2.7: Filtered acceleration time history

Figure 2.8 shows various frequency contributions with a clear peak occurring at the fundamental frequency of the bridge.

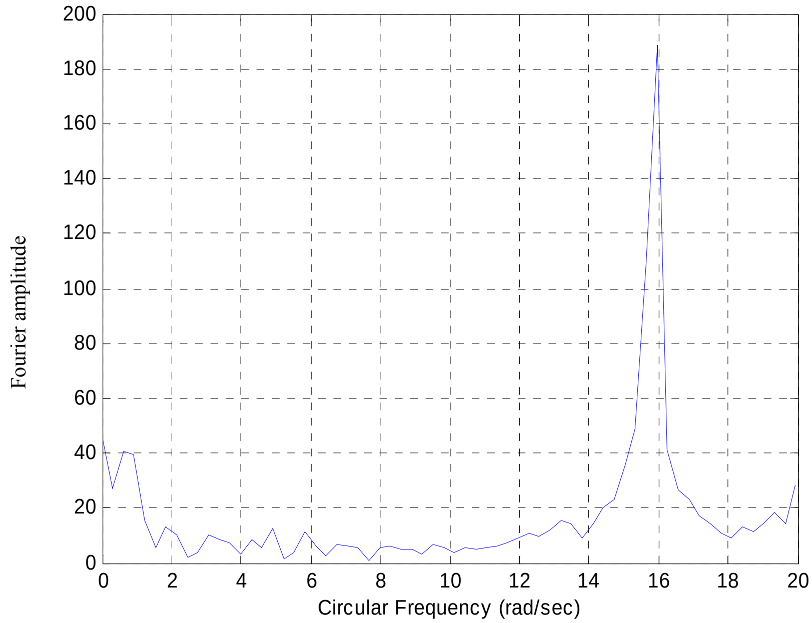

Figure 2.8: Frequency contributions of acceleration

The corresponding natural frequencies are listed in Table 2.1.

	Fundamental Circular Frequency of the Truss, ω
Vertical Direction	19.6 rad / sec
Horizontal Direction Parallel to Traffic Lanes	18.4 rad / sec
Horizontal Direction Perpendicular to Traffic Lanes	9.8 rad / sec

Table 2.1: Measured fundamental circular frequencies of the sign support truss

A similar procedure is used to obtain a symmetric and anti-symmetric bridge frequency contribution. The symmetric response is found by adding the unfiltered acceleration datum from the two truss columns. The resulting data is analyzed using the procedures described previously and the fundamental frequency of the symmetric response is obtained. This fundamental frequency corresponds to a vertical translational motion.

The anti-symmetric response is obtained by subtracting the unfiltered acceleration datum from the two truss columns. This resulting data is analyzed using the procedures described above and the fundamental frequency of the anti-symmetric response is obtained. This frequency corresponds to a fundamental frequency of the torsional motion. The corresponding natural frequencies are listed in Table (2.2).

	Fundamental Circular Frequency of the Bridge, ω
Translational Mode	15.95 rad / sec
Torsional Mode	18.4 rad / sec

Table 2.2: Measured fundamental circular frequencies of the bridge

2.9 Laboratory Fatigue Testing

The failed truss structure was subjected to fatigue testing in the Structures Laboratory of Case Western Reserve University. In order to fit into the available laboratory space, and also to remove the highly stressed and/or failed end portions of the truss, just under 10 feet was removed from each end of the truss, reducing its span to approximately 55 ft. The shorter truss was subjected to a vertical cyclic load, applied through an MTS dynamic actuator at midspan, such that the axial stress produced in all the diagonals was approximately 1 ksi. This level of stress is above the AASHTO specified constant amplitude fatigue limit (CAFL) of .44 ksi for the chord/diagonal welded joint, and hence should produce a fatigue failure within feasible testing periods. The truss is shown in the laboratory in Figure 2.9.

Figure 2.9: Laboratory test setup

A fatigue failure was initiated at 3,000,000 test cycles in the testing program at a chord/diagonal welded connection, as expected. The resulting fatigue crack is shown in Figure 2.10; the crack had begun its circumferential path around the chord section, just as the in-service field failure had progressed.

Figure 2.10: Crack initiated in laboratory testing

Chapter III

Finite Element Model of the Truss/Bridge Structural System

3.1 Sign Support Truss Finite Element Model

3.1.1 Model Description:

As the first part of the analysis, a finite element model of the aluminum three dimensional sign support truss was constructed. This model consists of 197 elements and 528 DOF's. The truss spans 73 ft longitudinally with a 22 ft clearance and its four main chords are arranged on a 4 ft square-sided configuration. The truss model is pinned in all connections except for those connecting it fixed to the bridge (see Figure 3.1). The aluminum truss chord members are 4.75" O.D. and 4.25" I.D.; the aluminum truss diagonals are 1.875" O.D. and 1.50" I.D. The steel tower legs are 6" SCH 80 and the steel tower diagonals are 2" SCH 40.

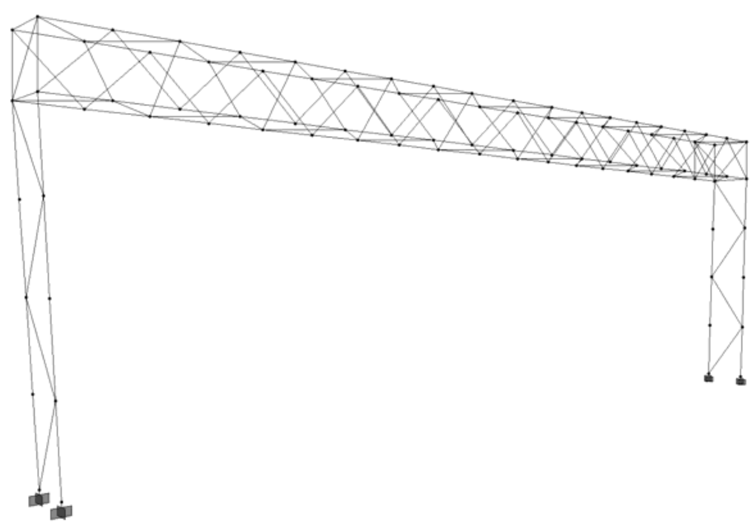

Figure 3.1: Sign support truss finite element model

3.1.2 Modal Analysis Results:

The modal analysis is performed on the truss model to determine the correlation of the fundamental frequencies of the model to the frequencies obtained from field data. The results are shown in Table 3.1.

	Fundamental Circular Frequency of the Truss Model, ω	Measured Fundamental Circular Frequency of the Truss, ω
Vertical Direction (z)	21.91 rad / sec	19.6 rad / sec
Horizontal Direction Parallel to Traffic Lanes (x)	18.93 rad / sec	18.4 rad / sec
Horizontal Direction Perpendicular to Traffic Lanes (y)	8.12 rad / sec	9.8 rad / sec

Table 3.1: Fundamental circular frequencies of the sign support truss

The comparison between the finite element results and field data shows a reasonable correlation and validates the model in representing the general dynamic behavior of the actual truss. The difference between the two can be attributed to the discrepancy in boundary conditions between the FE model and the actual truss. The model assumes rigid end supports, while the actual structure is supported elastically by the bridge structure. Also, the welded joint connections within the truss impose some constraint on relative rotation between members, which is not modeled.

3.1.3 Axial Force Results:

Element axial forces were obtained from the FE model for the three fundamental modes of vibration at their normalized amplitudes. It was found that the highest axial forces in the diagonal members are induced when the truss is subjected to the vertical mode shape displacement. However, the amplitude of the various modes in service is dependent on the excitation (see Figure 3.2).

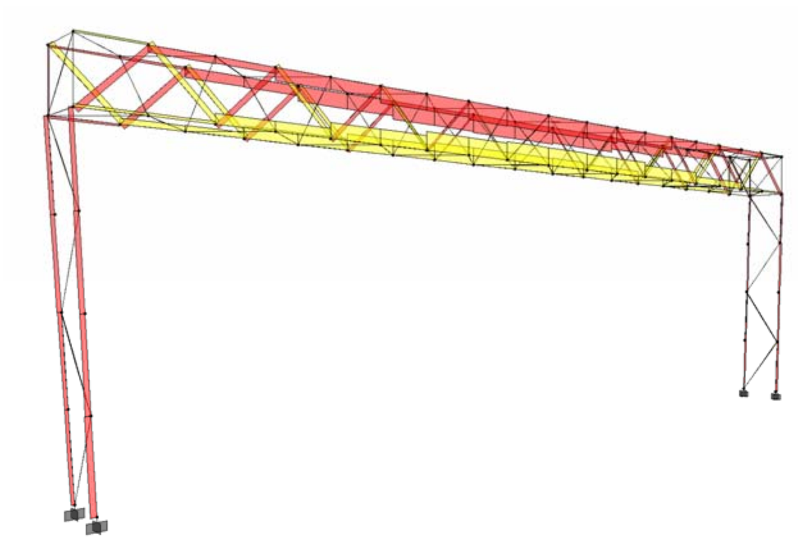

Figure 3.2: Axial forces associated with the vertical mode shape

This analysis also indicates that the largest forces in the diagonal members occur at the two ends of the truss, which is the locations of the observed fracture failure, indicating that vibrations in the vertical direction have likely contributed to the failure.

3.2 Finite Element Model of the Supporting Bridge

3.2.1 Model Description:

For the second part of the analysis, a finite element model of the truss-supporting bridge was constructed. This model consists of 418 frame elements, 969 solid elements, 1440 shell elements, with the total of 14259 DOF's.

3.2.2 Geometric Description:

This 484 ft. long model consists of 4 spans and is supported by five piers that are modeled as pin supports. This finite element system models a segment of the bridge between two thermal expansion joints, in which the truss was actually located.

3.2.3 Material Specifications:

The bridge model consists of concrete and steel materials. A 4 ksi normal weight concrete, with an elastic modulus of 3600 ksi, was used for the 8.5 in slab, modeled with solid elements (see Figure 3.3).

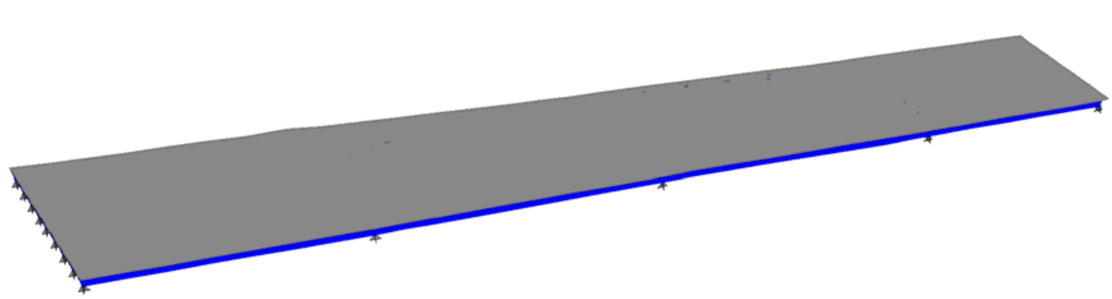

Figure 3.3: Concrete bridge slab

Typical construction grade steel with an elastic modulus of 29000 ksi was used for the 66 in deep girders, which vary in number along the bridge length due to the transition to the off-ramp. The first 1.5 spans, starting from the northern end of the bridge, are supported by seven girders. The next 2 spans are supported by eight girders and the last 1.5 spans are supported by nine girders. The girders are modeled with plate/shell elements (see Figure 3.4).

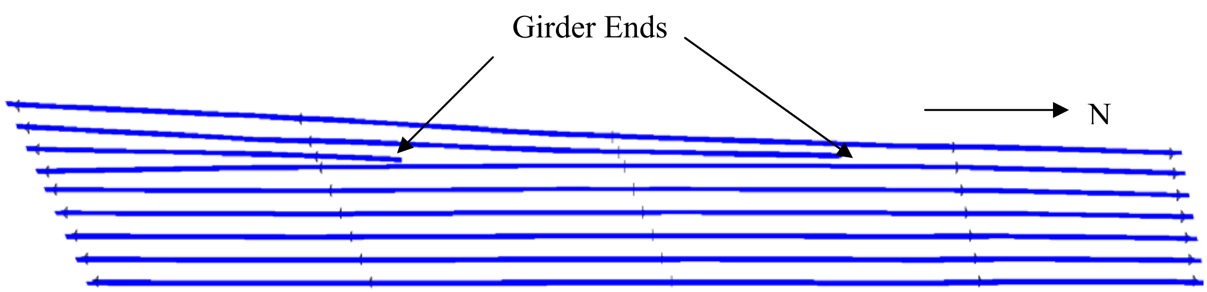

Figure 3.4: Steel bridge girder configuration

The steel diaphragms, or cross frames, were modeled as frame elements between girders (see Figure 3.5).

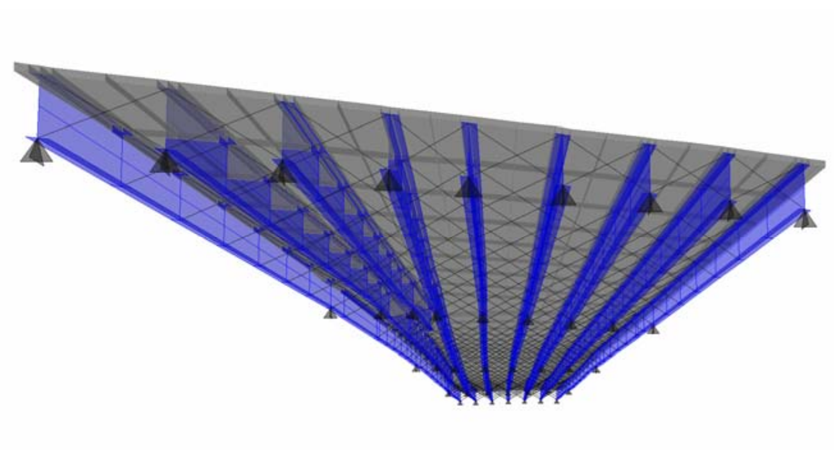

Figure 3.5: Bridge diaphragms

3.2.4 Traffic Pattern Description:

The bridge consists of three southbound traffic lanes, with a 60 mph speed limit. The inside lane proceeds straight throughout the bridge; the center lane separates into two lanes, one diverging to the right and one proceeding straight; the outside lane diverges to the right. Figure 3.6 shows the bridge model and the point of lane divergence.

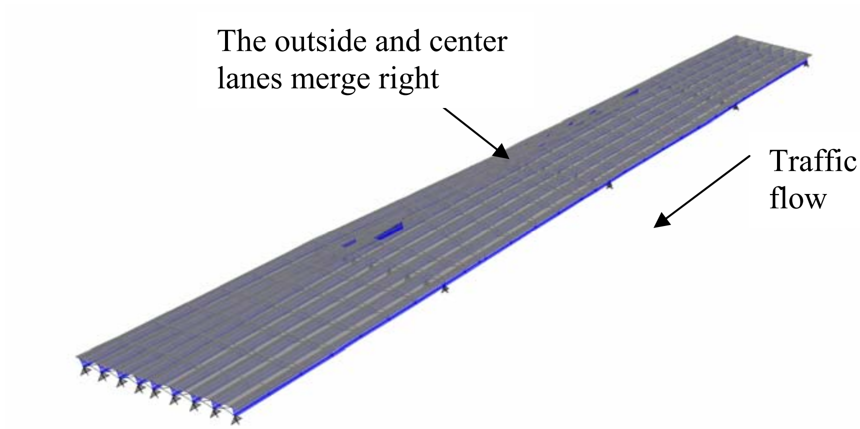

Figure 3.6: Truss supporting bridge finite element model

3.2.5 Modal Analysis Results:

The modal analysis was performed on the bridge model to determine the correlation of the fundamental frequencies of the model to the frequencies obtained from field data. The results are shown in Table 3.2.

	Fundamental Circular Frequency of the Bridge Model, ω	Measured Fundamental Circular Frequency of the Bridge, ω
Fundamental Mode	16.04 rad / sec	15.95 rad / sec
Translational Mode of the Truss Location	22.32 rad / sec	15.95 rad / sec
Torsional Mode of the Truss Location	21.85 rad / sec	18.4 rad / sec

Table 3.2: Fundamental circular frequencies of the bridge

The fundamental mode of the bridge is shown in Figure 3.7.

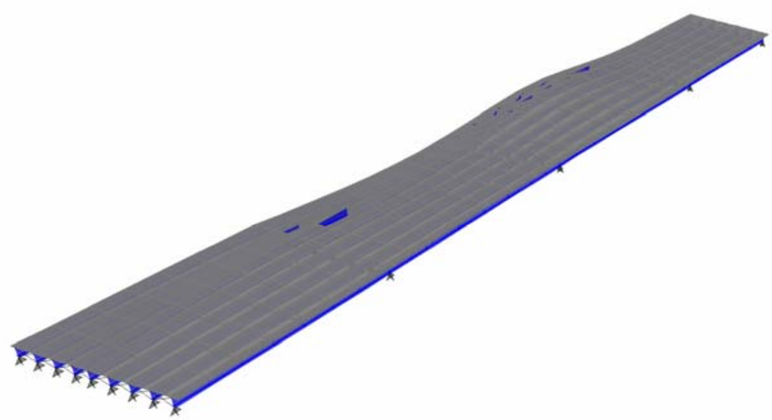

Figure 3.7: Fundamental mode shape of the bridge

The vertical and torsional modes at the bridge cross section where the truss is supported are shown in Figure 3.8 and 3.9 respectively.

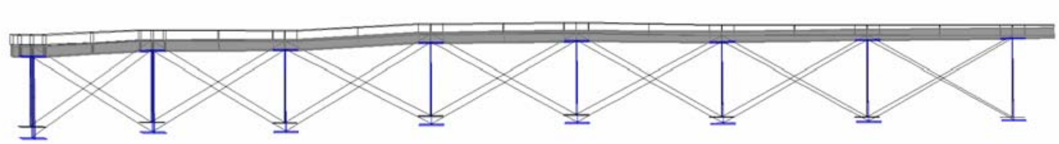

Figure 3.8: Vertical mode at the truss location

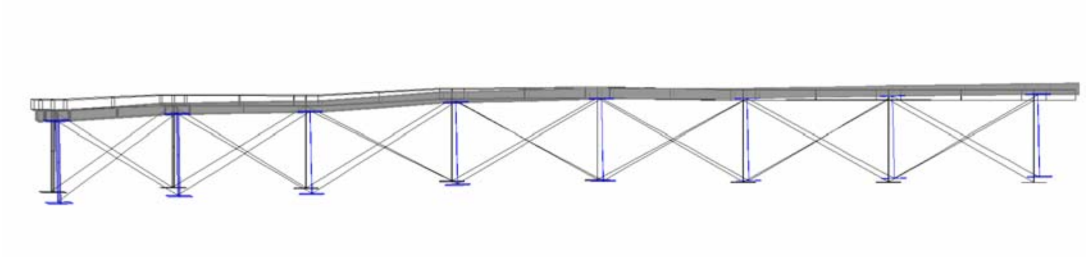

Figure 3.9: Torsional mode at the truss location

An analysis of the fundamental mode was conducted to determine the expected stress distribution pattern on the bridge. Two areas of stress concentration located near the girder ends (see Figure 3.4) were found, as shown in Figure 3.10.

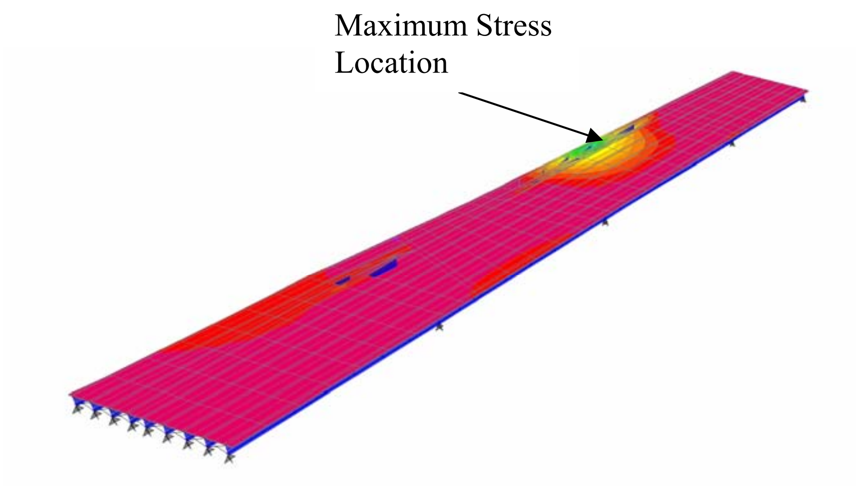

Figure 3.10: Maximum stress distribution of the bridge slab in the fundamental mode

The diaphragms were also analyzed for any unusual load distribution in the bridge fundamental mode. It was found that the maximum axial forces are located near the girder ends and near the piers (see Figure 3.11).

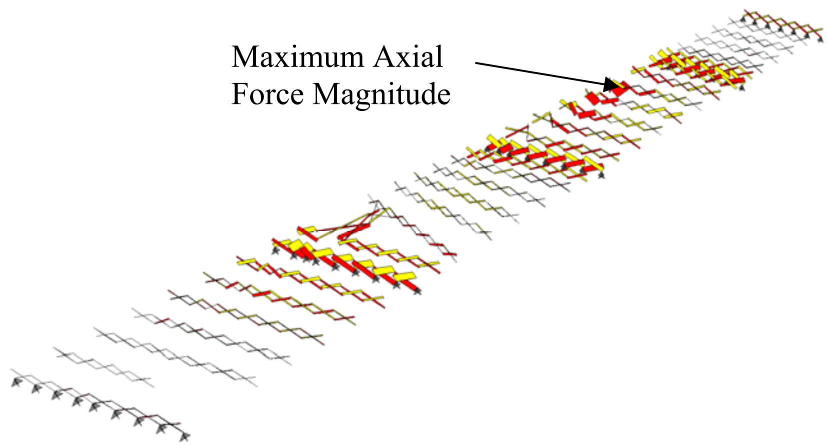

Figure 3.11: Axial forces in diaphragms in the fundamental mode

Figures 3.10 and 3.11 indicate that the girder terminations are areas of stress concentration in the bridge structure.

3.2.6 Self Weight Analysis Results:

The locations of the maximum stresses produced in the concrete slab due to dead load were checked. The resulting stress distribution is uniform except near the piers, with a maximum stress of 0.5 ksi (see Figure 3.12).

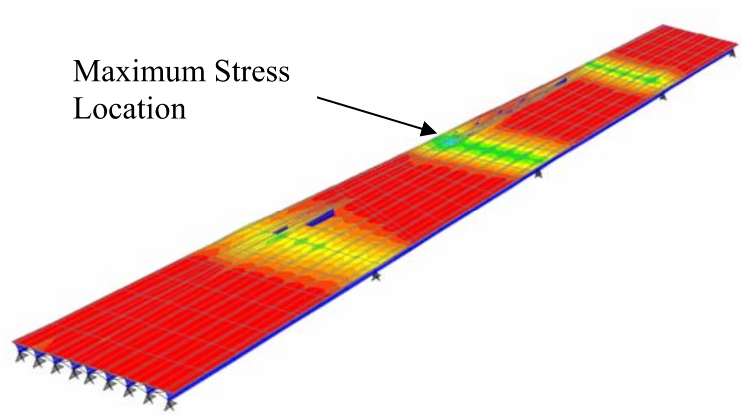

Figure 3.12: Maximum stress distribution in the bridge slab due to dead load

3.3 Truss/Bridge System Finite Element Model

3.3.1 Model Description:

For the third part of the analysis, a finite element model of the truss/bridge system was constructed (see Figure 3.13). This model consists of 615 frame elements, 969 solid elements, 1440 shell elements, contains 14799 DOF's and contains the same material and geometric properties as the previous separated models.

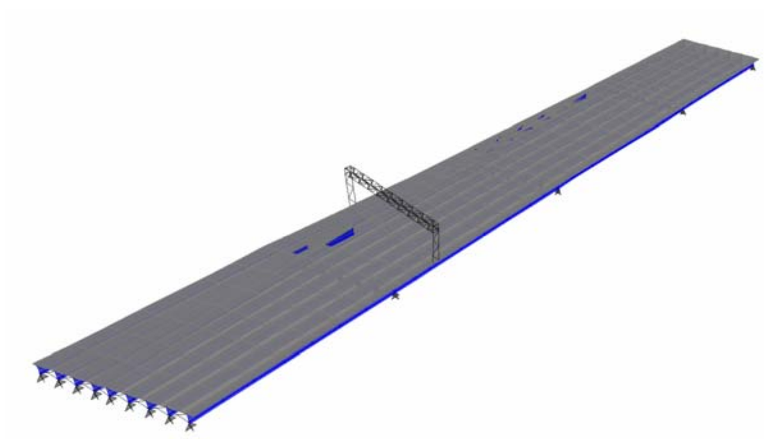

Figure 3.13: Finite element model of the truss/bridge system

3.3.2 Loading:

Five different types of loading were considered to model the effects of the dynamic loads on the truss. These load types, described in the following sections, are: galloping, vortex shedding, truck-induced wind gusts, natural wind load, and traffic loads.

3.3.2.1 Galloping:

Galloping is a form of dynamic wind response which arises to the varying angle of wind attack on the structure. This angle variation is caused by across-wind oscillation of the structure. When the motion of the structure is parallel to the direction of the wind flow the oscillation becomes larger. Galloping is most common in structures with high flexibility and low damping such as ice-covered cables or cantilever sign supports. Even though the effects of galloping can cause significant forces on a structure, they generally do not affect cylindrical members. Since the investigated truss is entirely made of cylindrical members, and reasonably high in natural frequency, the galloping phenomenon was not considered further.

3.3.2.2 Vortex Shedding:

Vortex shedding is another form of wind load. This phenomenon occurs when a structure is subjected to a steady uniform wind flow. The flowing wind produces an alternating pattern of shed vortices behind the element, causing it to oscillate in a direction normal to the wind flow. In the investigated truss the natural frequencies are again high enough that resonance with the vortex shedding phenomenon is not expected, and therefore the phenomenon is not considered further.

3.3.2.3 Truck-Induced Wind Gusts:

Forces due to truck-induced wind gusts are caused by the passage of the truck underneath the truss. As the truck passes, the induced wind flow collides with the roadway sign, causing oscillation. These wind loads are noticeable but for the purpose of this analysis they were neglected, since the truck-induced wind gust load is expected to be much smaller than the natural wind load.

3.3.2.4 Natural Wind Load:

The natural wind load was considered in the modeling of the structure. The wind load was modeled as a distributed equivalent static load found using an empirical relation given as:

$$q(ppf) = 0.00256 \cdot V_{\max}^2 \ (mph) \cdot D(ft) \cdot DragCoeficient \tag{45}$$

where, q is the equivalent distributed static load, $V_{\max}$ is the expected maximum velocity of the wind and D is the member's diameter. The drag coefficient for a circular member, at Reynolds Numbers expected in practice, is typically taken as 0.45. The maximum wind velocity considered was 100 mph and the corresponding wind force was calculated for all members in the truss (see Figures 3.14 and 3.15).

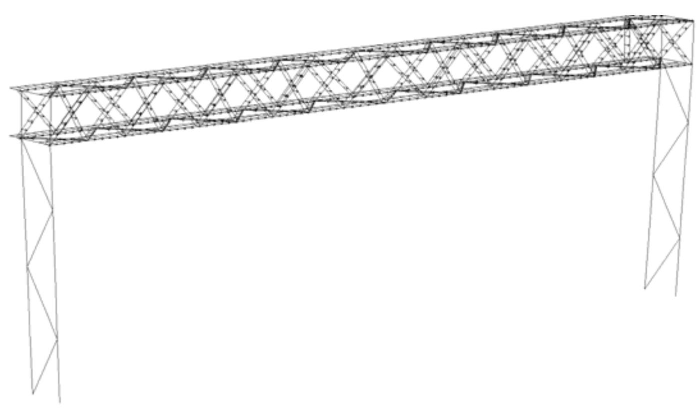

Figure 3.14: Truss wind load

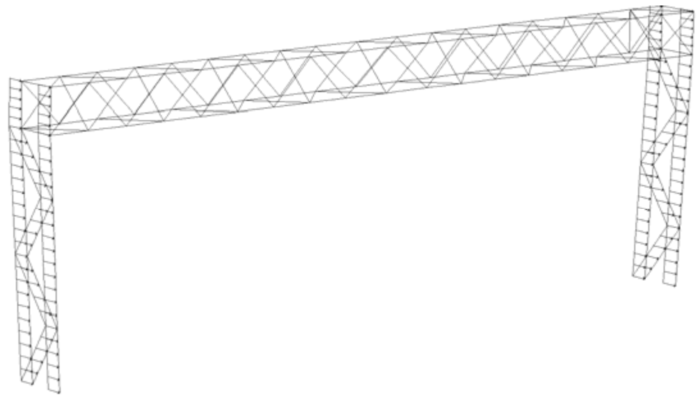

Figure 3.15: Truss support wind load

3.3.2.5 Traffic Load:

The dynamic traffic load is considered as a moving load, modeled by a single passage of an HS20 design truck, with the distance between the rear and center axles of 22 ft (see Figure 3.16).

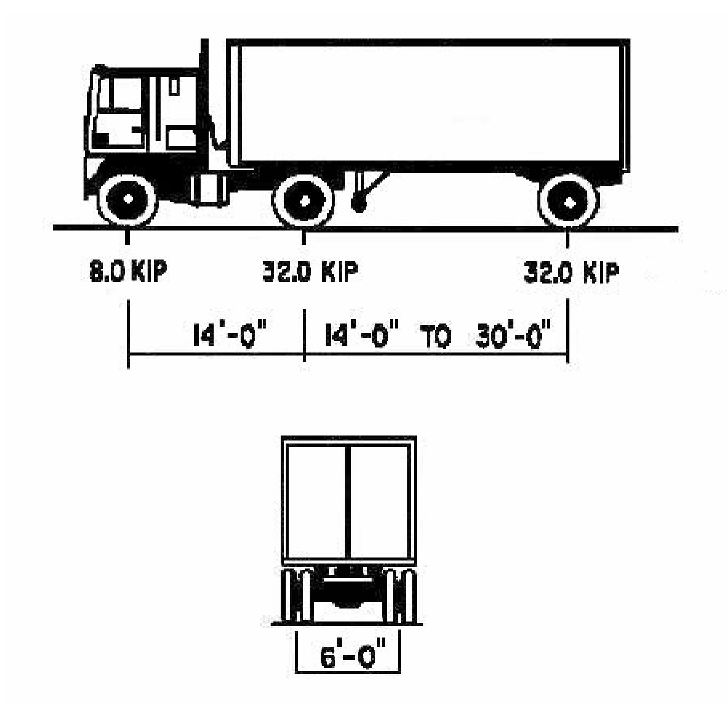

Figure 3.16: HS20 truck used to model traffic load

3.3.3 Time History Function:

Each axle of the truck is represented by a different triangular time history function at a set of nodes, scaled according to the axle load. The truck axle load was distributed laterally over four nodes, since the distance between nodes in the model did not correspond to the assumed axle spread. A typical time history function of a truck passing through a node is shown in Figure 3.17.

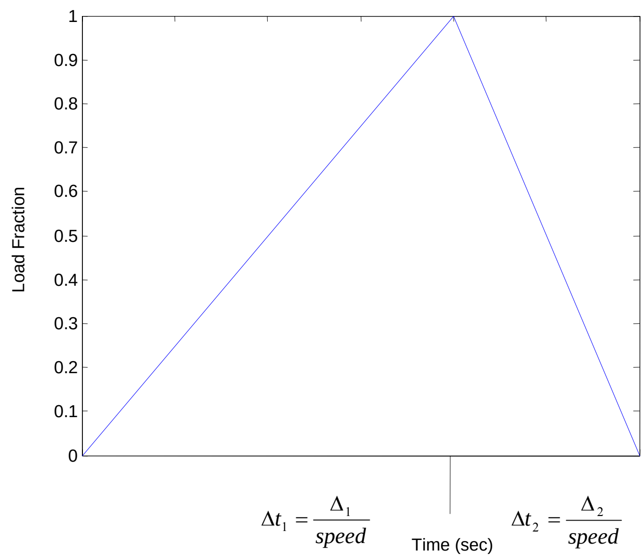

Figure 3.17: Time function of a truck passing through a node

The load fraction varies from 0 to 1, where 0 represents the truck passing over the previous or following node and 1 represents the truck passing over the node at which the function is defined. The truck's arrival time at different nodes is:

$$t_{i+1} = \frac{\Delta}{speed} + t_i \tag{46}$$

where, t_{i+1} is the arrival time of the truck at node $(i+1)$, t_i is the arrival time at node i, and Δ is the distance between nodes $(i+1)$ and (i).

3.3.4 Truck Speed:

The total of nine different truck passages is considered in the model. A truck passage at each of the three lanes is considered with three different speeds at each lane. The three truck passage speeds are; 55 mph, 60 mph, 65 mph, which were chosen based on the 60 mph speed limit. Since the outer lane causes a more non-symmetric response, it was modeled as merging to the right, while the center lane was modeled straight (see Figure 3.18).

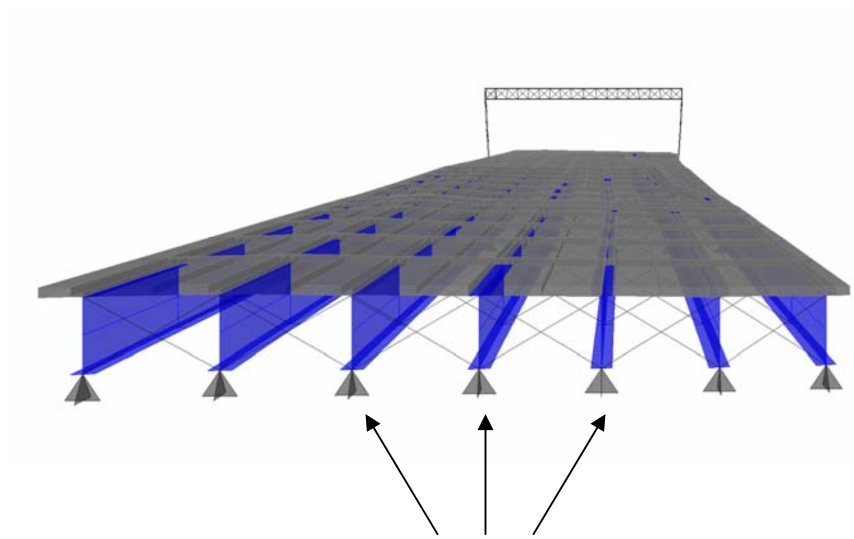

Figure 3.18: Three truck passage lanes

Chapter IV

Analysis Results and Conclusions

4.1 Finite Element Analysis Results

4.1.1 Wind Load Analysis Results:

The effects of the wind load on the sign support truss have been studied by performing an equivalent linear static analysis using SAP2000 software. The results obtained by the analysis show that the wind load does not produce any significant axial forces on the truss (see Figure 4.1).

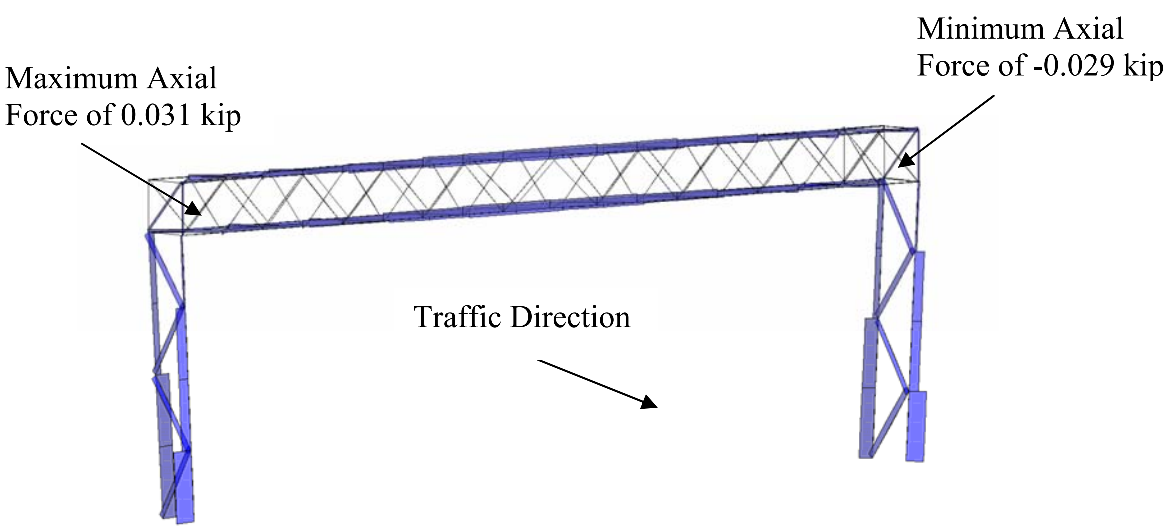

Figure 4.1: Axial force distribution in the sign support truss due to wind load in the traffic direction

Figure 4.2 shows the axial force distribution for the wind load in the direction opposite to the traffic flow.

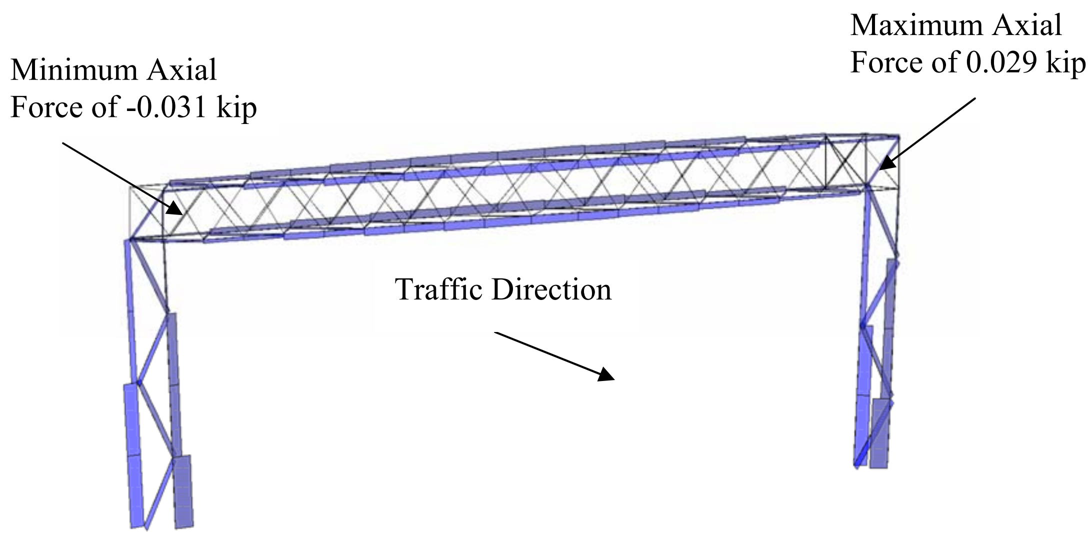

Figure 4.2: Axial force distribution in the sign support truss due to wind load in the direction opposite of traffic

The maximum and minimum axial forces in the diagonal members of the truss for each case are located near the edges of the truss. The stresses induced by axial forces are summarized in Table 4.1.

Loading Type	Maximum Stress (ksi)	Minimum Stress (ksi)
Wind Load in the Traffic Direction	0.0227	-0.0212
Wind Load in the Direction Opposite to Traffic	0.0212	-0.0227

Table 4.1: Maximum and minimum stresses due to wind load

The equivalent static wind-induced stresses in the diagonal members of the truss are small enough such that the wind load did not cause the truss failure.

4.1.2 Traffic Load Time History Analysis:

The effects of the moving traffic load on the sign support truss have been studied by performing a FE time history analysis. The damping ratio of the bridge/truss structural system was assumed to be 0.5%. From the preliminary analysis of the truss model, subjected to a vertical support motion, such as that one due to traffic loading, it was observed that the maximum axial forces in the diagonal members occur at the ends of the truss. Therefore, the time history of axial forces for two end diagonals was the primary load effect studied in the investigation. These two members exhibit the largest axial force range (see Figure 4.3).

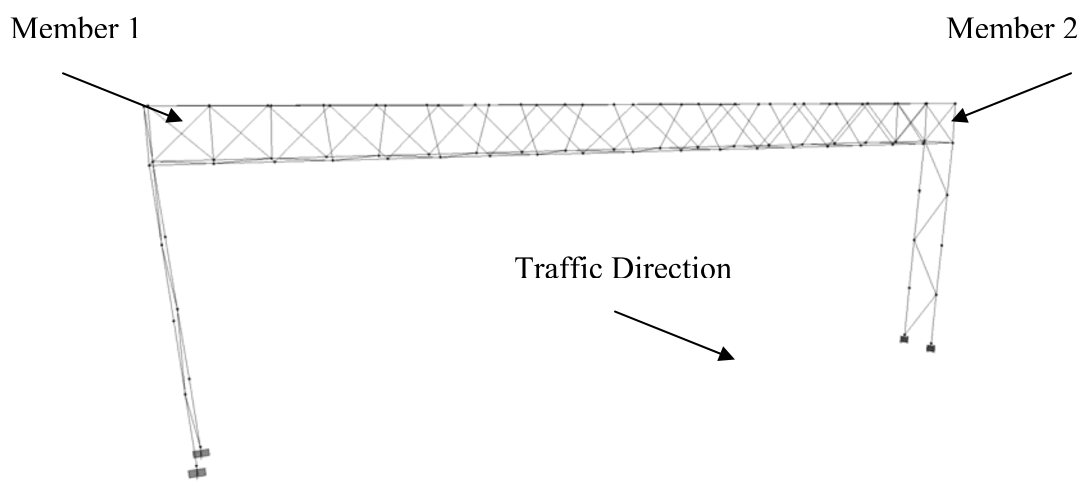

Figure 4.3: Truss members monitored during time history analysis

4.1.2.1 Axial Force Time History of Member 1:

Figures 4.4 to 4.6 show the results of the time history of Member 1 due to an inside lane truck passage at various speeds.

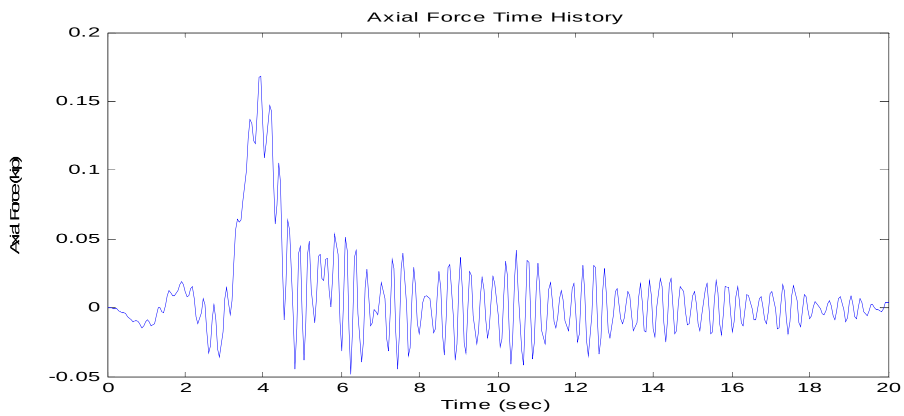

Figure 4.4: Member 1 force time history for the inside lane truck passage at 55 mph

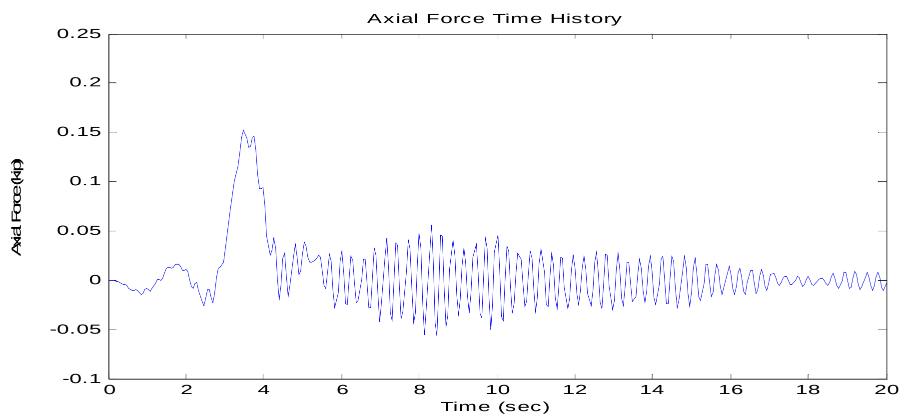

Figure 4.5: Member 1 force time history for the inside lane truck passage at 60 mph

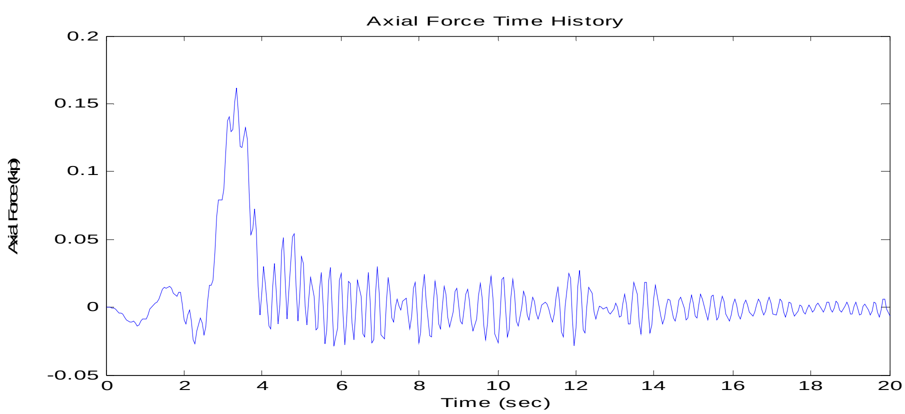

Figure 4.6: Member 1 force time history for the inside lane truck passage at 65 mph

Figures 4.7 to 4.9 show the results of the time history of Member 1 due to a center lane truck passage at various speeds.

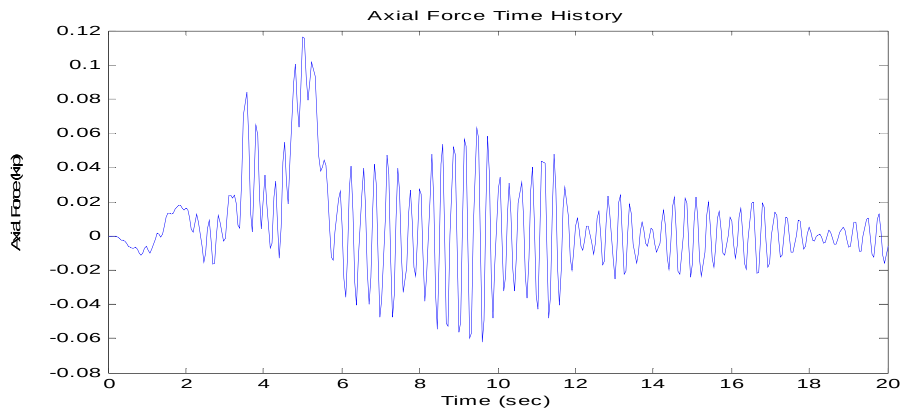

Figure 4.7: Member 1 force time history for the center lane truck passage at 55 mph

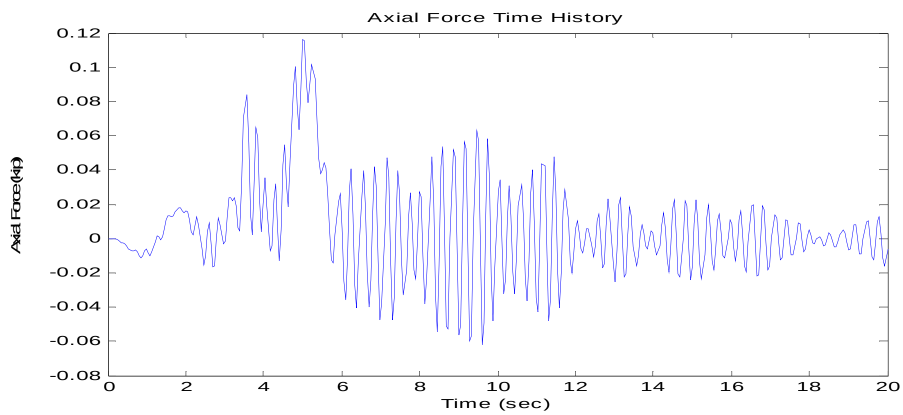

Figure 4.8: Member 1 force time history for the center lane truck passage at 60 mph

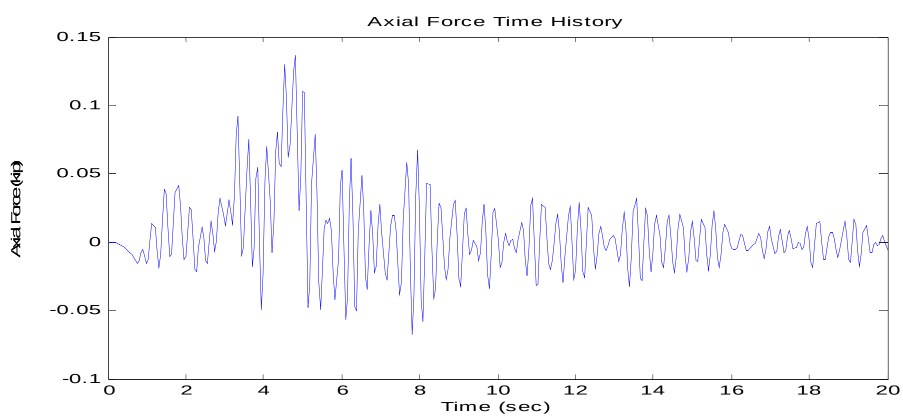

Figure 4.9: Member 1 force time history for the center lane truck passage at 65 mph

Figures 4.10 to 4.12 show the results of the time history of Member 1 due to outside lane truck passage at various speeds.

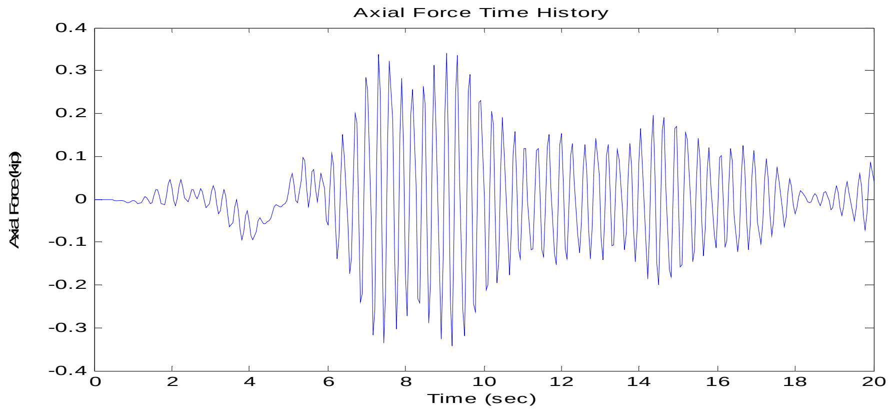

Figure 4.10: Member 1 force time history for the outside lane truck passage at 55 mph

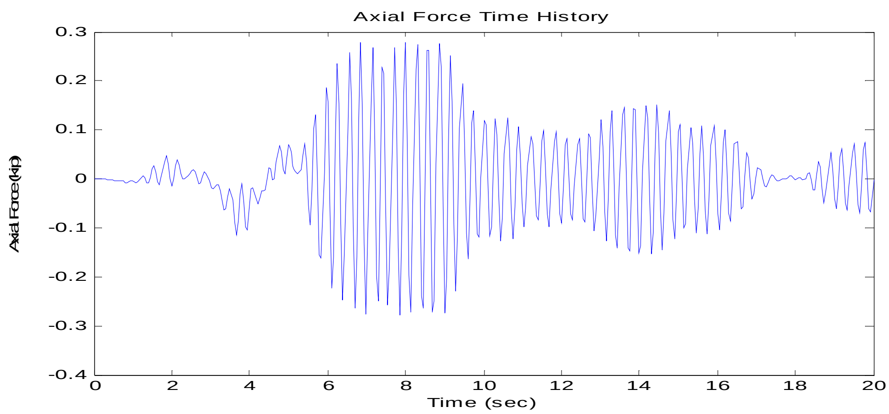

Figure 4.11: Member 1 force time history for the outside lane truck passage at 60 mph

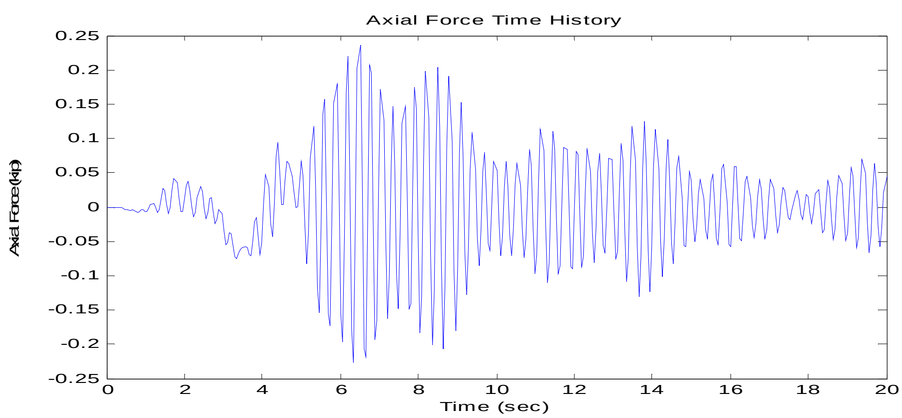

Figure 4.12: Member 1 force time history for the outside lane truck passage at 65 mph

4.1.2.2 Axial Force Time History of Member 2:

Figures 4.13 to 4.15 show the results of the time history of Member 2 due to the inside lane truck passage at various speeds.

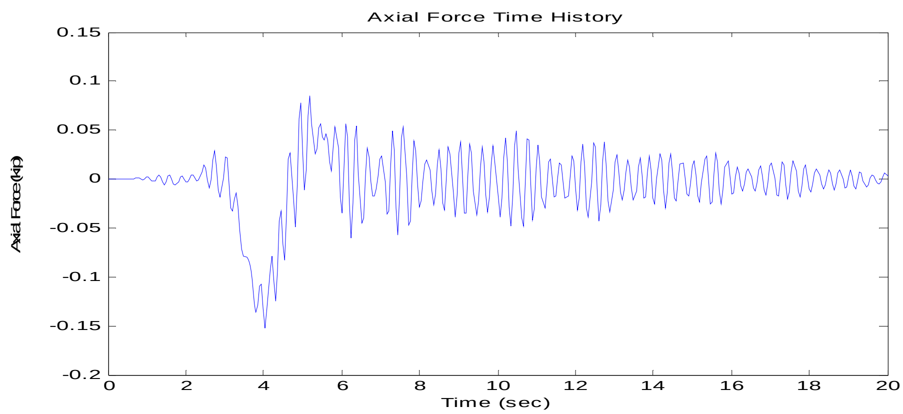

Figure 4.13: Member 2 force time history for the inside lane truck passage at 55 mph

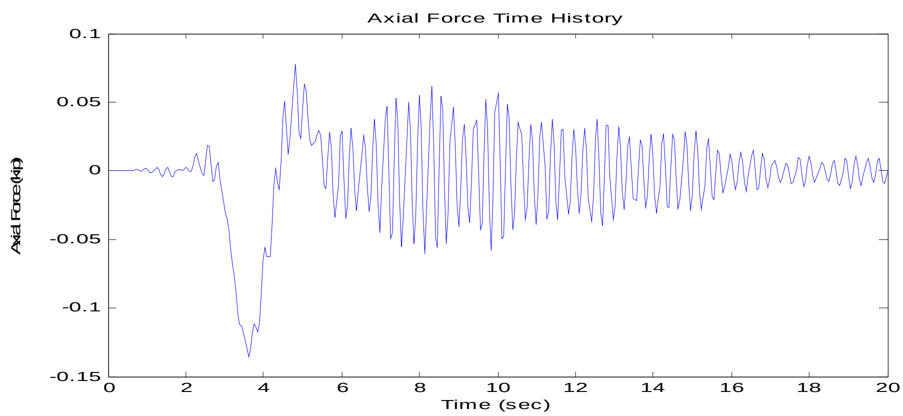

Figure 4.14: Member 2 force time history for the inside lane truck passage at 60 mph

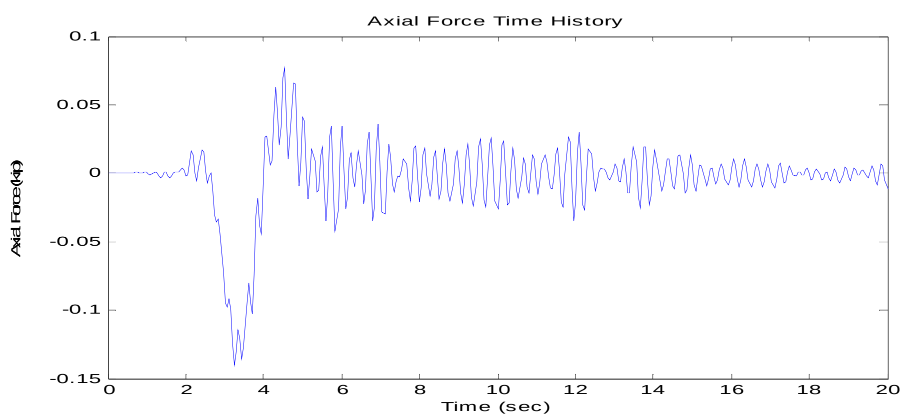

Figure 4.15: Member 2 force time history for the inside lane truck passage at 65 mph

Figures 4.16 to 4.18 show the results of the time history of Member 2 due to a center lane truck passage at various speeds.

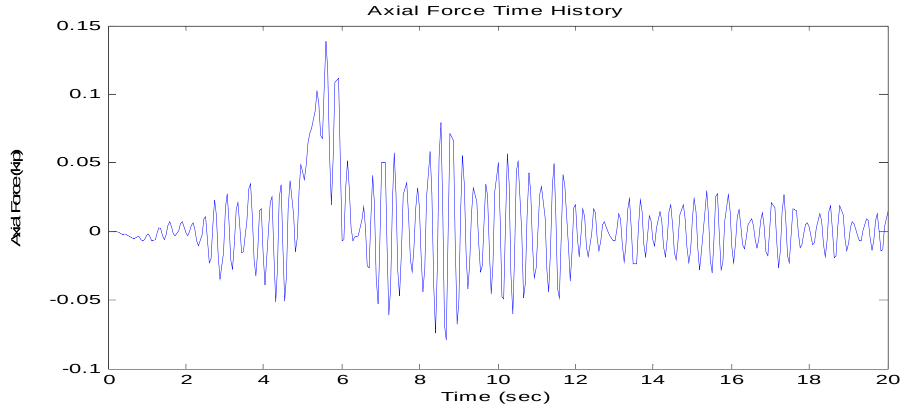

Figure 4.16: Member 2 force time history for the center lane truck passage at 55 mph

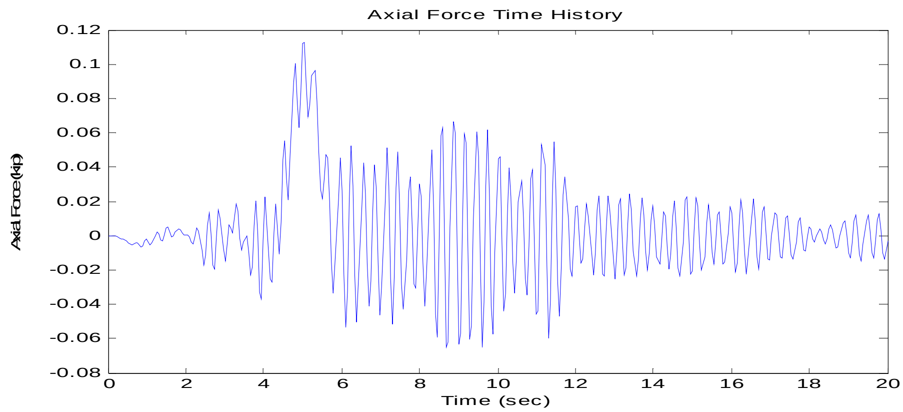

Figure 4.17: Member 2 force time history for the center lane truck passage at 60 mph

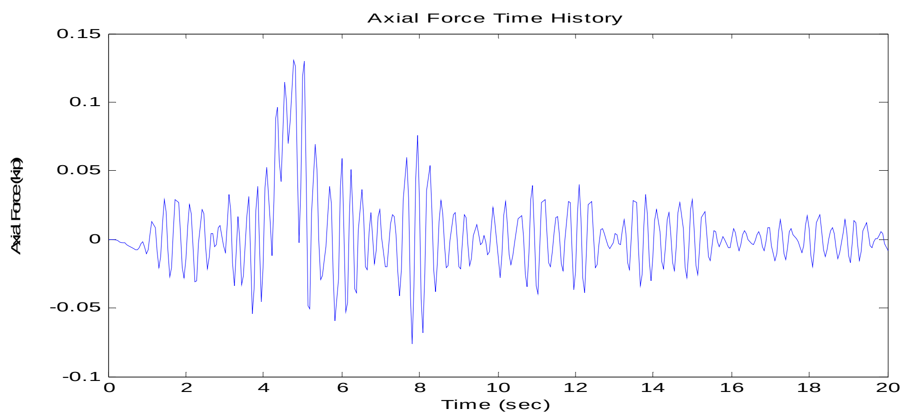

Figure 4.18: Member 2 force time history for the center lane truck passage at 65 mph

Figures 4.19 to 4.21 show the results of the time history of Member 2 due to an outside lane truck passage at various speeds.

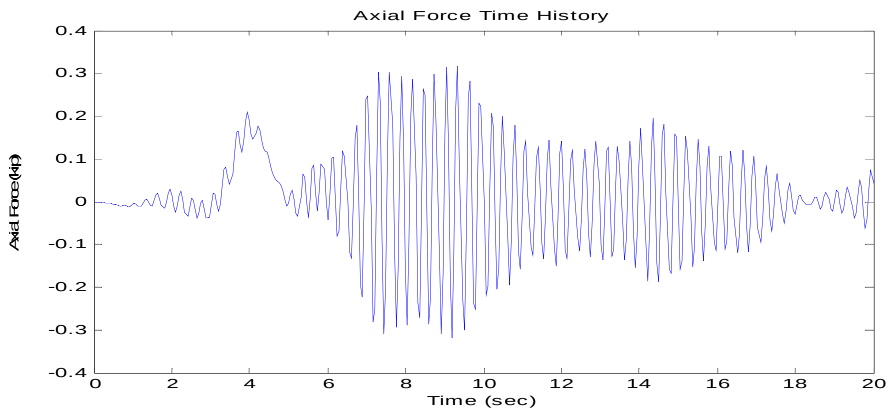

Figure 4.19: Member 2 force time history for the outside lane truck passage at 55 mph

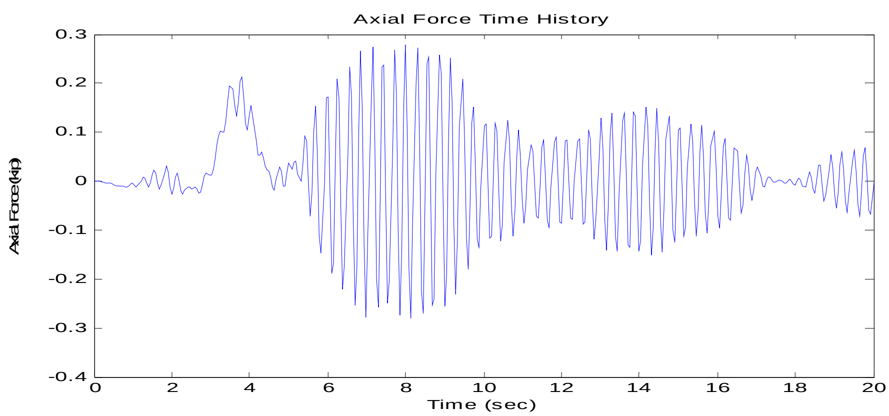

Figure 4.20: Member 2 force time history for the outside lane truck passage at 60 mph

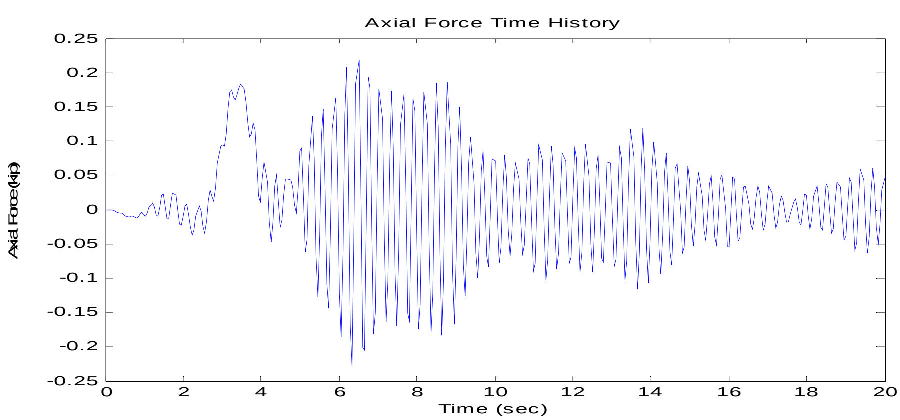

Figure 4.21: Member 2 force time history for the outside lane truck passage at 65 mph

4.2 Sign Support Truss Lifetime Analysis

The analysis of the expected lifetime for the sign support truss was performed using the results obtained from the finite element analysis. To best estimate a lifetime for the truss, the following stress range/number of cycles to failure relationship was used, which is an analytical approximation of a traditional (S-N) curve:

$$N_f = \frac{C_f}{S_R^3} \tag{47}$$

where N_f is the number of cycles to failure, S_R is the stress range, and C_f is a constant dependent on the material and weld detail. For the truss aluminum weld detail ET, $C_f = 1{,}870{,}000$. The plotted S-N for the aluminum ET welded detail and the observed laboratory experimental fatigue failure point mentioned in Chapter II is shown in Figure 4.22.

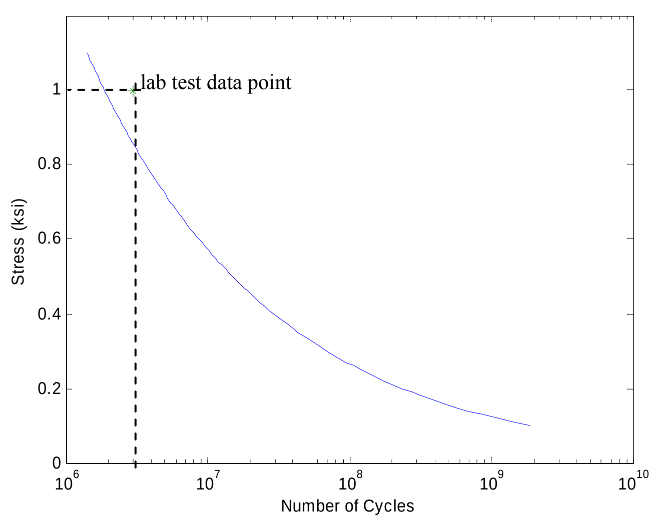

Figure 4.22: (S-N) curve for the ET aluminum weld detail

The laboratory testing corresponds reasonably well with the assumed curve.

4.2.1 Time History Fatigue Evaluation:

The axial force time history was used to determine the root mean cube stress range, S_{rmc}, using Miner's Rule and the number of cycles of stress variation per truck passage. According to the Miner's Rule, damage D can be defined as:

$$\sum_{i=1}^{m} D_i = \sum_{i=1}^{m} \frac{n_i}{N_i} \tag{48}$$

where, n_i is the number of cycles at stress S_i and N_i is the number of cycles to failure at stress S_i. Failure occurs when $\sum_{i=1}^{m} D_i = 1$. The damage created by a set of unequal stress ranges is considered to be equal to the damage created by an equivalent constant amplitude stress range, S_{rmc}, with an equal number of total stress cycles, $\sum_{i=1}^{m} n_i$:

$$\sum_{i=1}^{m} \frac{n_i}{N_i} = \frac{\sum_{i=1}^{m} n_i}{N_{rmc}} \tag{49}$$

where, N_{rmc} is the number of cycles to failure at stress S_{rmc}. From (S-N) curve:

$$N_{rmc} \cdot S_{rmc}^3 = C = N_i \cdot S_i^3 \tag{50}$$

then:

$$\sum_{i=1}^{m} \frac{n_i}{N_i} = \sum_{i=1}^{m} \frac{S_i^3 \cdot n_i}{C} = \frac{S_{rmc}^3}{C} \cdot \sum_{i=1}^{m} n_i \tag{51}$$

Therefore,

$$S_{rmc} = \left(\frac{\sum_{i=1}^{m} S_i^3 \cdot n_i}{\sum_{i=1}^{m} n_i} \right)^{1/3} \tag{52}$$

The root mean cube stress range results for Member 1 are shown in Table 4.2.

Lane of Passage	Truck Speed (mph)	Number of Cycles per Truck Pass	S_{rmc} (ksi)
	55	96	0.056
Inside Lane	60	97	0.055
	65	96	0.038
	55	97	0.060
Center Lane	60	99	0.052
	65	94	0.055
	55	99	0.287
Outside Lane	60	96	0.231
	65	107	0.175
Average	60	98	0.112

Table 4.2: The root mean cube stress deviation and the number of cycles of stress variation per truck passage for Member 1

The root mean cube stress range results for Member 2 are shown in Table 4.3.

Lane of Passage	Truck Speed (mph)	Number of Cycles per Truck Pass	S_{rmc} (ksi)
	55	97	0.055
Inside Lane	60	99	0.058
	65	95	0.038
	55	94	0.064
Center Lane	60	98	0.056
	65	93	0.055
	55	96	0.298
Outside Lane	60	98	0.252
	65	101	0.196
Average	60	97	0.119

Table 4.3: The root mean cube stress range and the number of cycles of stress variation per truck pass for Member 2

The results of induced stress range in members 1 and 2 show that the highest value occurs when the outside lane bridge traffic merges right onto interstate route 480. This fact results from the torsional effects of the traffic load, because of the asymmetric cross section of the bridge and the eccentric loading condition. The analysis of the truck passing on the center and inside lanes show much smaller stress variation. The speed analysis shows that the highest stresses occur at the slowest speed (55 mph). Both members have experienced a similar stress variation for all the loading patterns considered in the analysis. This shows that the fatigue failure has a nearly equal probability of occurrence at either end of the truss.

4.2.2 Analysis Results:

The lifetime of a member in terms of truck passages is calculated as:

$$Lifetime = \frac{N_f}{365 \cdot N_{Trucks} \cdot N_{Cycles}} \tag{53}$$

where $Lifetime$ is calculated in years, N_{Trucks} is the number of truck passages per day and N_{Cycles} is the number of cycles of stress deviation per truck passage. The results of the analysis for each truck passage with the assumed value of $N_{Trucks} = 200$ are shown in Tables 4.4 and 4.5 for members 1 and 2, respectively.

Lane of Passage	Truck Speed (mph)	Lifetime (years)
	55	1510
Inside Lane	60	1624
	65	4698
	55	1225
Center Lane	60	1811
	65	1607
	55	11
Outside Lane	60	22
	65	45
Average	60	187

Table 4.4: Lifetime of member 1 for each truck passage

Lane of Passage	Truck Speed (mph)	Lifetime (years)
	55	1624
Inside Lane	60	1350
	65	4748
	55	1049
Center Lane	60	1479
	65	1624
	55	10
Outside Lane	60	16
	65	34
Average	60	156

Table 4.5: Lifetime of member 2 for each truck passage

The actual lifetime analysis was based on two combinations of truck passages. Combination 1 involves 50%, 25% and 25% of trucks passing on the outside, center and inside lane, respectively. Combination 2 involves 33.3% of trucks passing on each lane considered in the model. The various truck speeds were divided equally among the respective lane passages. The results of the lifetime analysis of members 1 and 2 for combinations 1 and 2 are shown in Table 4.6 and 4.7, respectively.

	S_{rmc} (ksi)	Lifetime (years)
Member 1	0.192	37
Member 2	0.204	31

Table 4.6: Lifetime of members 1 and 2 for Combination 1

	S_{rmc} (ksi)	Lifetime (years)
Member 1	0.168	55
Member 2	0.179	46

Table 4.7: Lifetime of members 1 and 2 for Combination 2

The actual lifetime of the members was calculated using the average stress range from the analysis results of the two combinations (Table 4.8).

	Effective RMC Stress Range (ksi)	Lifetime (years)
Member 1	0.180	45
Member 2	0.192	37

Table 4.8: Actual lifetime of members 1 and 2

4.3 Conclusions

The analysis of the sign support truss subjected to dynamic loads shows that the traffic load was the main cause of the fatigue failure of the welded truss joint. The failure mechanism occurs primarily due to torsionally induced stresses caused by eccentric slow moving heavy traffic load. This occurred because the torsional frequency of the bridge approaches the vertical frequency of the truss. Therefore, the load exciting the torsional mode induces the highest stresses in the truss. The lifetime of member 2 was shown to be 37 years, which is approximately the lifetime of the actual failure. The lifetime of member 1, which did not fail, is higher than that of member 2.

4.4 Recommendations

The lifetime of the truss can be increased by enhancing the truss capacity or its location on the bridge, or by utilizing a steel truss rather than an aluminum truss.

- To accommodate the range of axial forces in the diagonal members of the truss, a larger aluminum cross section could be used to decrease the induced stresses. A decreased stress range would greatly increase the lifetime of the truss members;

increasing the cross section by 30%, for example, would increase the expected lifetime of the weld detail to 83 years.

- The lifetime of the truss can also be increased by relocating it to the piers, where there will be negligible induced support vibration due to traffic load.
- The sign could also be relocated to the part of the bridge with a more symmetrical cross section that has less torsional motion, as the torsional bridge mode was closest in natural frequency to the natural vibration modes of the truss.
- The sign support truss could be fabricated from steel, which does tend to exhibit an endurance limit, below which fatigue life is presumably unlimited.

4.5 Future Work

The failure investigation of the truss could be examined in a greater detail by analyzing and studying the welded joint using finite element modeling of the weld region. A more detailed analysis would allow for a better understanding of the internal forces in the vicinity of the crack which occurred due to traffic loading. A fracture analysis might also be performed and checked with the microscopic investigation of the weld so that the failure mechanism can be better understood.

There is also a need to address the issue of traffic induced vibrations of bridge-mounted sign supports. Current AASHTO standards for sign support structures do not provide any guidance on the issue. Although not affecting the majority of sign support structures, such load environments can easily present a safety issue for the traveling public, as was the case for this structure.

BIBLOGRAPHY

1. Huckelbridge, Arthur A., 2005. “ Advanced Steel Design-Fatigue ”. Class-notes ; Case Western Reserve University.

2. Huckelbridge, Arthur A., Gasparini, Dario, Mullen, Robert, 2003. “ The Dynamic Load Environment of Bridge-Mounted Sign Support Structures ”. Case Western Reserve University. Student Study Submitted to the Ohio Department of Transportation.

3. Huckelbridge, Arthur A., Kafali, Cagdas and Gilmore, David., 2002. “ Implementation of Filed Strain Measurements for Fatigue Lifetime Evaluation ”. Case Western Reserve University. Sate Job No. 14745(0).

4. Gasparini, Dario., 2004. “ Structural Dynamics ”. Class-notes ; Case Western Reserve University.

5. Oppenheim, Alan V. and Shafer, Ronald W., 1975. “ Digital Signal Processing ”. Massachusetts Institute of Technology and Georgia Institute of Technology.

6. Newland D. E., 1975. “ Random Vibrations and Spectral Analysis ”. University of Cambridge.

7. Barsom, John M. and Rolfe, Stanley T., 1977. “ Fracture & Fatigue Control in Structures, Application of Fracture Mechanics ”. Second Edition. United States Steel Corporation and University of Kansas.

8. Jones D. R. H., 1998. “ Failure Analysis Case Studies ”. University of Cambridge.

9. Kaczinski, M. R., Dexter, R. J. and Van Dien J. P., 1996. “ Fatigue-Resistant Design of Cantilever Signal, Sign and Light Supports ”. ATLSS Engineering Research Center and Lehigh University.

10. McDonald, James R., Kishor, Mehta C., Oler, Walter W. and Pulipaka, Narendra, 1995. “ Wind Load Effects on Signs, Luminaires and Traffic Signal Structures ”. Texas Tech University. Report 13031F.

11. Pantelides, Chris P. and Nadauld, Justin, 2004. “ Fatigue Tests of Cracked and GFRP-Repaired Aluminum Overhead Structures ”. University of Utah. TRB 2004 Annual Meeting.

12. Fouad, Fouad H. and Calvert, Elizabeth, 2004. “ Impact of the New Wind Load Provisions on the Design of Structural Supports ”. University of Alabama at Birmingham. TRB 2004 Annual Meeting.

13. Ahlborn, Theresa M., van de Lindt, John W. Uzcategui, Alonso J., Lewis, Matthew E., 2004. " Cost and Performance Comparison of the Nation's Overhead Sign Support Structures ". Michigan Technological University. TRB 2004 Annual Meeting. TRB Paper No. 04-2574.

14. PCB Piezotronics, Inc., 1993. " Vibration & Shock Sensor Selection Guide, Piezoelectric Accelerometers ".